Measurement report: Atmospheric nitrate radical chemistry in the South China Sea influenced by the urban outflow of the Pearl River Delta

Jie Wang[1, 2], Haichao Wang[1, 2 *], Yee Jun Tham[3, 4 *], Lili Ming[5], Zelong Zheng[1], Guizhen Fang[3], Cuizhi Sun[1, 2], Zhenhao Ling[1, 2], Jun Zhao[1, 2], Shaojia Fan[1, 2]

[1] School of Atmospheric Sciences, Sun Yat-sen University, and Southern Marine Science and Engineering Guangdong Laboratory (Zhuhai), Zhuhai, 519082, China
[2] Guangdong Provincial Observation and Research Station for Climate Environment and Air Quality Change in the Pearl River Estuary, Key Laboratory of Tropical Atmosphere-Ocean System (Sun Yat-sen University), Ministry of Education, Zhuhai, 519082, China
[3] School of Marine Sciences, Sun Yat-sen University, Zhuhai 519082, China.
[4] Pearl River Estuary Marine Ecosystem Research Station, Ministry of Education, Zhuhai, 519082, China.
[5] Technical Center of Gongbei Customs District of China, Zhuhai, 519000, China.

Correspondence to: Haichao Wang (wanghch27@mail.sysu.edu.cn); Yee Jun Tham (thamyj@mail.sysu.edu.cn)

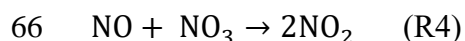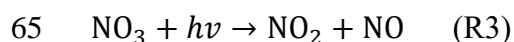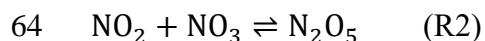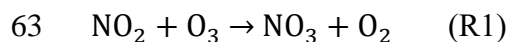**Abstract.** Nitrate radical (NO_3) is a critical nocturnal atmospheric oxidant in the troposphere, which widely affects the fate of air pollutants and regulates air quality. Many previous works have reported the chemistry of NO_3 in inland regions of China, while fewer studies target marine regions. Here, we present a field measurement of the NO_3 reservoir, dinitrogen pentoxide (N_2O_5), and related species at a typical marine site (Da Wan Shan Island) located in the South China Sea in the winter of 2021. Two patterns of air masses were captured during the campaign, including the dominant airmass from inland China (IAM) with a percentage of ~84%, and the airmass from eastern coastal areas (CAM) with ~16%. During the IAM period, the NO_3 production rate reached 1.6 ± 0.9 ppbv h^{-1} due to the transportation of the polluted urban plume with high NO_x and O_3. While the average nocturnal N_2O_5 and the calculated NO_3 mixing ratio were 119.5 ± 128.6 pptv and 9.9 ± 12.5 pptv, respectively, and the steady state lifetime of NO_3 was 0.5 ± 0.7 min on average, indicating intensive nighttime chemistry and rapid NO_3 loss at this site. By examining the reaction of NO_3 with volatile organic compounds (VOCs) and N_2O_5 heterogeneous hydrolysis, we revealed that these two reaction pathways were not responsible for the NO_3 loss (<20%), since the NO_3 reactivity (k(NO_3)) towards VOCs was small (5.2×10^{-3} s^{-1})

and the aerosol loading was low. Instead, NO was proposed to significantly contribute to nocturnal NO_3 loss at this site, despite the nocturnal NO concentration always at sub-ppbv level and near the instrument detection limit. It might be from the local soil emission or others. We infer that the nocturnal chemical NO_3 reactions would be largely enhanced once without NO emission in the open ocean after the air mass passes through this site, thus highlighting the strong influences of the urban outflow to the downwind marine areas in terms of nighttime chemistry. During the CAM period, nocturnal ozone was higher, while NO_x was much lower. The NO_3 production was still very fast, with a rate of 1.2 ppbv h^{-1}. With the absence of N_2O_5 measurement in this period, the NO_3 reactivity towards VOCs and N_2O_5 uptake were calculated to assess NO_3 loss processes. We showed that the average k(NO_3) from VOCs (56.5%, $2.6 \pm 0.9 \times 10^{-3}$ s^{-1}) was higher than that from N_2O_5 uptake (43.5%, $2.0 \pm 1.5 \times 10^{-3}$ s^{-1}) during the CAM period, indicating a longer NO_3/N_2O_5 lifetime than that during IAM period. This study improves the understanding of the nocturnal NO_3 budget and environmental impacts with the interaction of anthropogenic and natural activities in marine regions.

1. Introduction

Reactive nitrogen compounds, especially the nitrate radical (NO_3) and dinitrogen pentoxide (N_2O_5) play an essential role in nocturnal atmospheric chemistry (Wayne et al., 1991; Brown and Stutz, 2012). NO_3 is mainly generated via the oxidation of NO_2 by O_3 (R1), and then NO_3 further reacts with NO_2 to produce N_2O_5 (R2) with a thermal equilibrium. The temperature-dependent equilibrium constant, K_{eq}, regulates the equilibrium favoring NO_3 and NO_2 at higher temperatures (Osthoff et al., 2007; Chen et al., 2022). During daytime, the NO_3 mixing ratio is generally low as its lifetime is very short (< 5 s) due to the fast photolysis (R3) and rapid reaction with NO (R4) (a rate constant of 2.6×10^{-11} cm^3 molecule^{-1} s^{-1} at 298 K, Atkinson et al., 2004). While at night, NO_3 accumulates and can reach tens to hundreds of parts per trillion by volume (pptv), making it the major nocturnal oxidizing agent (Wang et al., 2015).

$$NO_2 + O_3 \rightarrow NO_3 + O_2 \quad \text{(R1)}$$

$$NO_2 + NO_3 \rightleftharpoons N_2O_5 \quad \text{(R2)}$$

$$NO_3 + h\nu \rightarrow NO_2 + NO \quad \text{(R3)}$$

$$NO + NO_3 \rightarrow 2NO_2 \quad \text{(R4)}$$

During nighttime, NO_3 is the most important oxidant for alkenes (Mogensen et al., 2015; Edwards et al., 2017), particularly in rural, remote, or forested environments, where it predominantly reacts with unsaturated biogenic volatile organic compounds (VOCs), especially isoprene and monoterpene (Ng et al., 2017; Liebmann et al., 2018b; Liebmann et al., 2018a), to form alkyl nitrates ($RONO_2$), that ultimately lead to secondary organic aerosols (SOAs) (Brown and Stutz, 2012). The observations and model simulations showed that the measured particulate organic nitrates were largely attributed to the nocturnal NO_3 oxidation across Europe (Kiendler-Scharr et al., 2016). The NO_3 oxidation was also reported to play an important role in aerosol formation in the Southeastern United States with high isoprene and monoterpene emissions (Xu et al., 2015). These studies highlighted the critical role of the reaction of NO_3 with VOCs in NO_3 budget and organic aerosol pollution. In addition, NO_3 also reacts with dimethyl sulfide (DMS) over the ocean, affecting the marine sulfur cycle and thus cloud formation and global climate (Aldener et al., 2006; Brown and Stutz, 2012; Ian Barnes et al., 2006; Rosati et al., 2022). While in high aerosol loading regimes, the N_2O_5 heterogeneous uptake becomes a significant indirect NO_3 loss pathway. The hydrolysis reaction produces nitrate (NO_3^-) and nitryl chloride ($ClNO_2$) on chloride-containing aerosol surfaces (Osthoff et al., 2008; Thornton et al., 2010), in which $ClNO_2$ activates the Cl radical and further enhances the photochemistry and ozone pollution in the following day (Riedel et al., 2012; Riedel et al., 2014; Behnke et al., 1993).

Different NO_3 loss pathways produce different air pollutants, thus characterization of NO_3 budget is essential to clarify the NO_3 chemistry in air pollution under various environments. Observations of N_2O_5 and NO_3 in different regions and evaluation of their loss processes have been reported in numerous studies (Crowley et al., 2011; Geyer et al., 2001; Brown et al., 2011; Dewald et al., 2022; Niu et al., 2022; Brown et al., 2016; Wang et al., 2020a; Tham et al., 2016; Aldener et al., 2006; Lin et al., 2022). In general, the NO_3 loss process shows significant regional differences. In urban areas featuring intensive anthropogenic NO_x emissions and moderate (or high) aerosol loading, N_2O_5 uptake is comparable or even dominates the NO_3 loss (Wang et al., 2013). While in rural and forested areas with abundant biogenic VOC (BVOC) emissions, the NO_3 loss processes were usually dominated by BVOCs (Dewald et al., 2022; Geyer et al., 2001; Brown et al., 2011). As for the coastal areas, which were jointly affected by the polluted air mass from the inland and the relatively clean air mass from the ocean, the dominant NO_3 loss process varies greatly depending on the air mass origin (Aldener et al., 2006; Niu et al., 2022; Brown et al., 2016; Crowley et al., 2011). For instance, Crowley et al. (2011) found in the Atlantic coast of Southern Spain (forested area) that when the air mass mainly originated from the Atlantic, NO_3 was mainly consumed by BVOCs (mainly monoterpenes) emitted from nearby forests, while when the air mass came from the continent, NO_3 loss was mainly due to reactions with anthropogenic

105   VOCs (AVOCs).

106   China has been recently proven to be a hot spot of nocturnal chemistry with a high NO_3
107   production rate (Wang et al., 2023). Many studies have reported the mechanisms, budget,
108   or impacts of NO_3-N_2O_5 chemistry in different regions, while most of them were conducted
109   in urban regions (Wang et al., 2013; Yan et al., 2021; Wang et al., 2020a; Wang et al., 2017c;
110   Wang et al., 2017d). For example, Wang et al. (2017b) showed a significant contribution
111   of N_2O_5 uptake to nitrate pollution in summer and winter, and they also highlighted the fast
112   organic nitrate production rate observed in Beijing rural region in summer (Wang et al.,
113   2018b). Only several studies focused on nighttime oxidation in coastal cities like Shanghai,
114   Shenzhen, and Hong Kong (Zhu et al., 2022; Niu et al., 2022; Yan et al., 2019), which
115   showed different patterns of NO_3 chemistry compared with urban regions. Even fewer field
116   studies were conducted on the island which is far away from the coastal cities where the
117   interactions of the oceanic atmosphere and urban plumes can significantly affect the NO_3
118   budget and impacts. Given the diversity of air masses in inland and coastal areas, studies
119   are needed to gain a comprehensive understanding of NO_3 losses in different atmospheric
120   environments, particularly in coastal and marine areas.

121   Therefore, we conducted an intensive field observation on Da Wan Shan Island (DWS) in
122   the winter of 2021, which is a typical island site in the north of the South China Sea, and
123   downwind of the city clusters in the Pearl River Delta, China during the winter monsoon
124   periods. The island features a subtropical oceanic monsoon climate, and the north and
125   northeast synoptic winds from inland PRD and eastern China coast are generally
126   predominant in winter (Liu et al., 2019; Wang et al., 2018a). This allows us to further
127   investigate the interactions between anthropogenic emissions and marine emissions from
128   the perspective of nighttime chemistry. In this study, the measurements of N_2O_5 and the
129   related species during the DWS winter campaign are reported. We have identified two types
130   of air masses from both mainland China and coastal areas. Finally, the NO_3 budget and loss
131   processes in different air masses are characterized.

132   **2. Methods**

133   **2.1 Site description**

134   The field campaign was conducted at Da Wan Shan Island (21°55′57″ N, 113°43′15″ E)
135   from Nov. 9th to Dec. 16th, 2021. Fig. 1 shows the location of the study site, which is
136   approximately 60 km southwest of Hong Kong; 40 km southeast of Zhuhai; and about 100
137   km and 80 km away from the megacities Guangzhou and Shenzhen, respectively. This
138   island is dominated by mountainous terrain with an area of 8.1 km^2 and has a small

population of about 3,000. Anthropogenic emissions are sparse and no industrial pollution sources were identified, though numerous ships engaging in local fishing activities were observed, potentially affecting the local atmosphere. During the measurement, local airflow was consistently from either the northwest or southeast (Fig. 1a) due to the winter monsoon, with wind speeds most frequently ranging from 1.8 to 7.9 m s^{-1} (10th - 90th percentiles) and an average of 4.5 ± 2.6 m s^{-1}. This wind direction is indicative of the mixing of air masses from both continental and coastal areas. The HYbrid Single-Particle Lagrangian Integrated Trajectory model (HYSPLIT) was adopted to investigate the historical trajectory. The HYSPLIT model was run for 48 hours backward in time at local times of 20:00, 24:00, and 04:00, and at a height of 70 m above sea level. It confirmed that the airmass during nighttime mostly came from inland China (fresh urban emissions, IAM, 84%) and the coastal areas (aged urban emissions, CAM, 16%). IAM featured the outflow from inland China, such as Guangzhou and Changsha, while CAM featured the outflow of coastal cities like Hong Kong and Shenzhen. No air masses free of pollution from the South China Sea were observed during the measurement period. All measurement instruments were placed in the DWS Atmospheric-Marine Research Station, located on the rooftop with inlets approximately 10 m above ground level and about 72 m above sea level. All times were given in CNST (Chinese National Standard Time = UTC + 8 h), with sunrise around 06:40 CNST and sunset at 17:40 CNST.
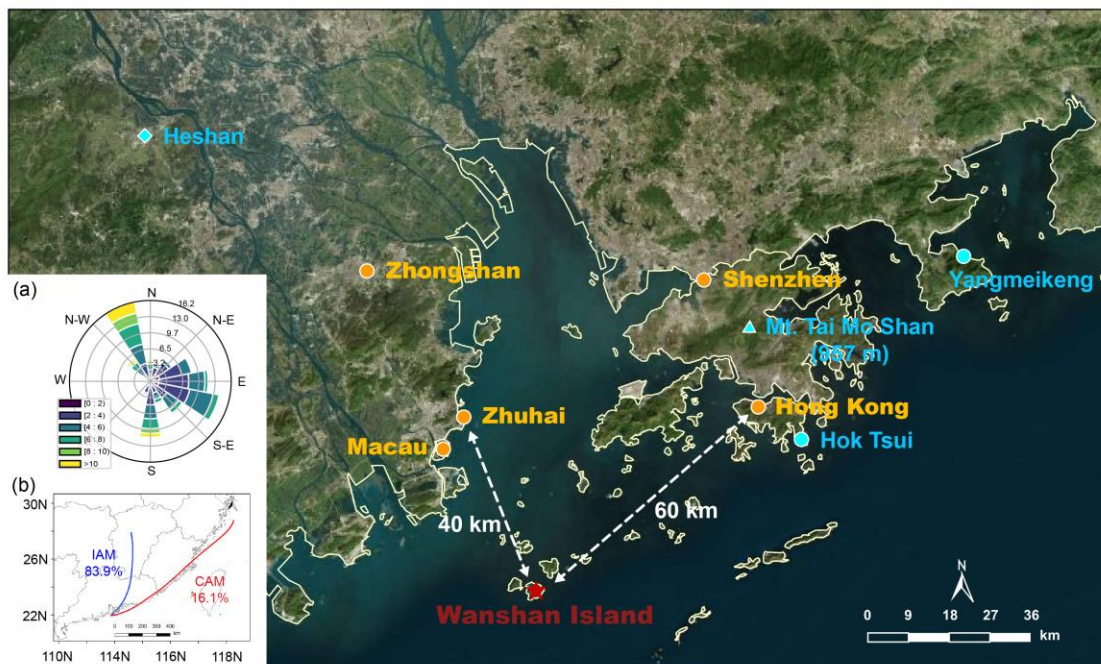
Figure 1. A map of the field measurement site of Wanshan Island (red star) and the surrounding environment (extracted from BingSatelliteMap). Two coastal sites Hok Tsui

161 (Yan et al., 2019) and Yangmeikeng (Niu et al., 2022), and an urban site Heshan (Wang et
162 al., 2022; Yun et al., 2018b) are denoted as blue circle and diamond, respectively. The blue
163 triangle denoted Mt. Tai Mo Shan (957 m), a mountainous site that studied the nighttime
164 chemistry in the nocturnal residual layer (Brown et al., 2016). The inset plot (a) provides
165 the wind rose for the sampling site during the campaign. Panel (b) shows the clustering
166 result of the 48-hrs backward trajectory calculations at nighttime using the HYSPLIT
167 model throughout the campaign.

168 **2.2 Instrument setup**

169 Various parameters were measured in this study, including N_2O_5, NO, NO_2, O_3, VOCs,
170 particle number size distribution (PNSD), and meteorological parameters with different
171 instruments. The detail information about these instruments is listed in Table 1. The N_2O_5
172 measurements were performed using a cavity-enhanced absorption spectrometer (CEAS)
173 which has been deployed in several field campaigns (Wang et al., 2017a; Wang et al., 2017b;
174 Wang et al., 2018b; Wang et al., 2020b). In brief, ambient N_2O_5 was thermally decomposed
175 to NO_3 in a perfluoro alkoxy alkane (PFA) tube (length: 35 cm, I.D.: 4.35 mm) heated to
176 130 °C, and NO_3 was detected within a 110 °C PFA resonator cavity. NO was injected to
177 destroy NO_3 from N_2O_5 thermal decomposition every 5 min cycle, and the result was used
178 as the reference spectrum to avoid the influence of ambient water vapor. A pair of high-
179 reflectivity (HR) mirrors (Layertec GmbH, Mellingen, Germany) with a diameter of 25.0
180 mm (C0.00/-0.10 mm) was used to enhance the effective optical pathlength. Mirror
181 reflectivity ($R(\lambda)$) was calibrated with high purity He and N_2 in the current experimental setup
182 during the field measurements. $R(\lambda)$ was calibrated to be 0.99997, and the effective pathlength
183 of the optical resonator was 13.96 km. A Teflon polytetrafluoroethylene (PTFE) filter was
184 used to remove ambient aerosol particles, and the inlet flow rate was 1.0 L·min^{-1}. The loss
185 of N_2O_5 in the sampling line and filter was considered in the data correction according to
186 previous work (Wang et al., 2017a). Here the CEAS measurement encompasses the
187 combined concentration of ambient $[N_2O_5 + NO_3]$ and effectively represents N_2O_5 under high
188 NOx (or low temperature) conditions when the NO_3-to-N_2O_5 ratio is likely to be low.
189 Accounting for the instrument's transmission efficiency and the thermal transformation
190 between NO_3 and N_2O_5, the contribution of NO_3 is sufficiently negligible in comparison to
191 N_2O_5. Nevertheless, we have taken it into account during the N_2O_5 data correction. The
192 limit of detection (LOD) was 2.7 pptv (1σ), and the measurement uncertainty was ± 19%.

193 **Table 1.** The information of observation instruments used during the DWS campaign.

Species	Techniques	Detection limit	Accuracy	Time resolution
N_2O_5	CEAS	2.7 pptv (1σ)	±19%	10 s

NO	Chemiluminescence	0.4 ppbv	$\pm 5\%$	1 min
NO$_2$	Chemiluminescence	0.4 ppbv	$\pm 5\%$	1 min
O$_3$	UV photometry	0.4 ppbv	$\pm 5\%$	1 min
VOCs	PTR-TOF-MS	0.01 ppbv	$\pm 10\%$	10 s
PNSD	SMPS	5–300 nm	$\pm 10\%$	5 min

194   NO$_x$ and O$_3$ were measured by commercial instruments (model T200U and model T400U,
195   Teledyne API Inc., respectively) calibrated with zero air before the measurement. The
196   nitrogen oxide analyzer uses the chemiluminescence detection method to measure the
197   original NO and converted NO$_2$, and the LOD was 0.4 ppbv for each species. Aerosol
198   surface area density (S$_a$, μm^2 cm^{-3}) was calculated based on the particle numbers and
199   geometric diameter, which was calculated through the results measured by a laboratory-
200   assembled scanning-mobility particle sizer (SMPS) according to Mcmurry et al. (2000).
201   This SMPS system consists of two differential mobility analyzers (DMA, "nano-DMA"
202   mode 3081A, and "regular-DMA" mode 3085A, TSI Inc.) in parallel, and a condensed
203   particle counter (mode 3787, TSI Inc.) as the detector. The combination of nano DMA and
204   conventional mode 3085A DMA enables the SMPS to have better detection performance
205   for particles below 50 nm. In this measurement, SMPS measured the particle size
206   distribution in 5-300 nm with a time resolution of 5 minutes, and Sa can be regarded as the
207   lower limit value. A growth factor $f(RH) = 1 + 8.8 \times (RH/100)^{9.7}$ (Liu et al., 2013) was used
208   here to correct dry state S$_a$ to wet state S$_a$.
209   VOCs were measured by proton transfer reaction time of flight mass spectrometry (PTR-
210   TOF-MS, Ionicon Analytik GmbH, Innsbruck, Austria) with a time resolution of 10 s. At
211   the end of this campaign, background measurements and instrument calibration were
212   conducted with high-purity nitrogen and multi-component VOC gas standards, respectively.
213   The instrument calibration results yielded strong linear relationships ($R^2 = 0.98$) between
214   the proton transfer reaction rate constants and the sensitivities of ten calibrants, including
215   acetaldehyde, acetone, dimethyl sulfide, isoprene, methyl ethyl ketone, benzene, toluene,
216   styrene, o-xylene, and trimethylbenzene. The sensitivities of the uncalibrated species were
217   determined through the rate constants of the proton transfer reactions and their correlation
218   coefficients with sensitivity. Meanwhile, the VOCs were also sampled by canister and
219   analyzed by a gas chromatograph equipped with a mass spectrometer or flame ionization
220   detector (GC-MS) for some ozone polluted days. For the absence of nocturnal data from
221   canister samples, the following analysis was based on the PTR-TOF-MS measurement
222   except the weight of α-pinene and β-pinene detected by GC-MS. Since monoterpene
223   species cannot be distinguished by PRT-TOF-MS, the reaction rate constant of the sum
224   monoterpene reaction with NO$_3$ was weighted by the campaign-averaged weight of α-
225   pinene and β-pinene detected by GC-MS. Meteorological parameters (i.e., temperature (T),

226 relative humidity (RH), wind speed, and wind direction) were routinely monitored with a
227 time resolution of 5 min.

228 **2.3 The calculation of NO₃ budget and lifetime**

229 With the observation of N_2O_5, NO_3 can be calculated according to their temperature-
230 dependent equilibrium relationship (Eq. 1) (Brown and Stutz, 2012). Lifetimes are
231 commonly expressed as the ratio of their concentrations to the NO_3 production rate as
232 determined by Eq. 2 and Eq. 3, assuming the production and loss are in dynamic balance
233 at night (Brown et al., 2003; Brown and Stutz, 2012). The production rate of nitrate radical,
234 $P(NO_3)$, is commonly expressed by Eq. 4, where $k_{NO_2+O_3}$ represents the temperature-
235 dependent reaction rate constant of NO_2 and O_3 (Atkinson et al., 2004). In general, the
236 nocturnal NO_3 losses typically include three main pathways (Eq. 5): (1) the reaction with
237 NO, (2) the reactions with VOCs, and (3) N_2O_5 uptake.

238 $[NO_3] = [N_2O_5]/Keq(T)[NO_2]$

239 $Keq = 5.50 \times 10^{-27} \times \exp(10724/T)$ (Eq. 1)

240 $\tau_{N_2O_5} = \dfrac{[N_2O_5]}{P(NO_3)} = \dfrac{[N_2O_5]}{k_{NO_2+O_3}[NO_2][O_3]}$ (Eq. 2)

241 $\tau_{NO_3} = \dfrac{[NO_3]}{P(NO_3)} = \dfrac{[NO_3]}{k_{NO_2+O_3}[NO_2][O_3]}$ (Eq. 3)

242 $P(NO_3) = k_{NO_2+O_3}[O_3][NO_2]$ (Eq. 4)

243 $L(NO_3) = \sum k_i[VOC_i][NO_3] + k_{NO+NO_3}[NO][NO_3] + k_{het}[N_2O_5]$ (Eq. 5)

244 The NO_3 reactivity towards VOCs, $k(NO_3)$, is the first-order loss rate coefficient calculated
245 from the products of the bimolecular rate coefficients k_i and the VOC concentrations as
246 shown in Eq. 6.

247 $k(NO_3) = \sum k_i[VOC_i]$ (Eq. 6)

248 The k_{het} is the first-order loss rate coefficient of N_2O_5 uptake on the aerosol surface. It
249 depends on the uptake coefficient $\gamma(N_2O_5)$, the aerosol surface area density Sa (μm^2 cm^{-3}),
250 and the mean molecular speed c (Eq. 7). The $\gamma(N_2O_5)$ is influenced by chemical
251 composition, physical properties of aerosol, as well as ambient conditions including related

252   humidity and temperature (Yu et al., 2020; Wagner et al., 2013; Wang et al., 2018b; Bertram
253   and Thornton, 2009; Tang et al., 2014; Kane et al., 2001). There are several kinds of
254   methods proposed to quantify or estimate $\gamma(N_2O_5)$ by using observed parameters. Given
255   that some essential parameters were not directly measured during this campaign, only two
256   approaches were employed to estimate the N_2O_5 uptake coefficient. The first method is the
257   pseudo steady state method by assuming that N_2O_5 and NO_3 have achieved a steady state
258   (Brown et al., 2009). $\gamma(N_2O_5)$ and k_{NO_3} can be determined from the slope and intercept of
259   linear regression of $K_{eq}[NO_2] \tau(N_2O_5)^{-1}$ versus $0.25cSaK_{eq}[NO_2]$ respectively as shown
260   in Eq. 8. The second is the parameterization method. As the aerosol compositions used to
261   estimate the N_2O_5 uptake coefficients were not measured, only a simplified
262   parameterization is available that based on relative humidity (RH) and temperature (Eq. 9)
263   (Hallquist et al., 2003; Kane et al., 2001; Evans and Jacob, 2005). Although simple, it had
264   an overall reasonable performance in China (Wang et al., 2022; Tham et al., 2018; Wang
265   et al., 2020a).

266    $$k_{het} = \frac{1}{4}cS_a\gamma(N_2O_5) \qquad (\text{Eq. 7})$$

267    $$K_{eq}[NO_2]\tau(N_2O_5)^{-1} = \frac{1}{4}cS_a\gamma(N_2O_5)K_{eq}[NO_2] + k_{NO_3} \quad (\text{Eq. 8})$$

268    $$\gamma(N_2O_5) = \alpha \times 10^\beta$$

269    $$\alpha = 2.79 \times 10^{-4} + 1.3 \times 10^{-4} \times RH - 3.43 \times 10^{-6} \times RH^2 + 7.52 \times 10^{-8} \times RH^3$$

270    $$\beta = 4 \times 10^{-2} \times (T - 294) \ (T > 282K)$$

271    $$\beta = -0.48 \ (T < 282K) \qquad (\text{Eq. 9})$$

272   **3.   Results and discussion**

273   **3.1 Measurement overview**

274   The time series of N_2O_5, related trace gases, and selected meteorological parameters for
275   the study period are depicted in Fig. 2. The air masses are categorized into IAM and CAM
276   according to the backward trajectories at 20:00, 00:00, and 04:00 each day as illustrated in
277   Fig. 1. The detailed information of two kinds of air masses is listed in Table 2. Data gaps
278   for N_2O_5 were caused by technical problems, mirror reflectivity calibration, or instrumental
279   maintenance, which usually took place in the daytime. In this campaign, meteorological

280   conditions featured a typical subtropical winter climate with average temperature and RH
281   values of 20.1 ± 1.9 °C and 52.0% ± 13.6%, respectively.

282
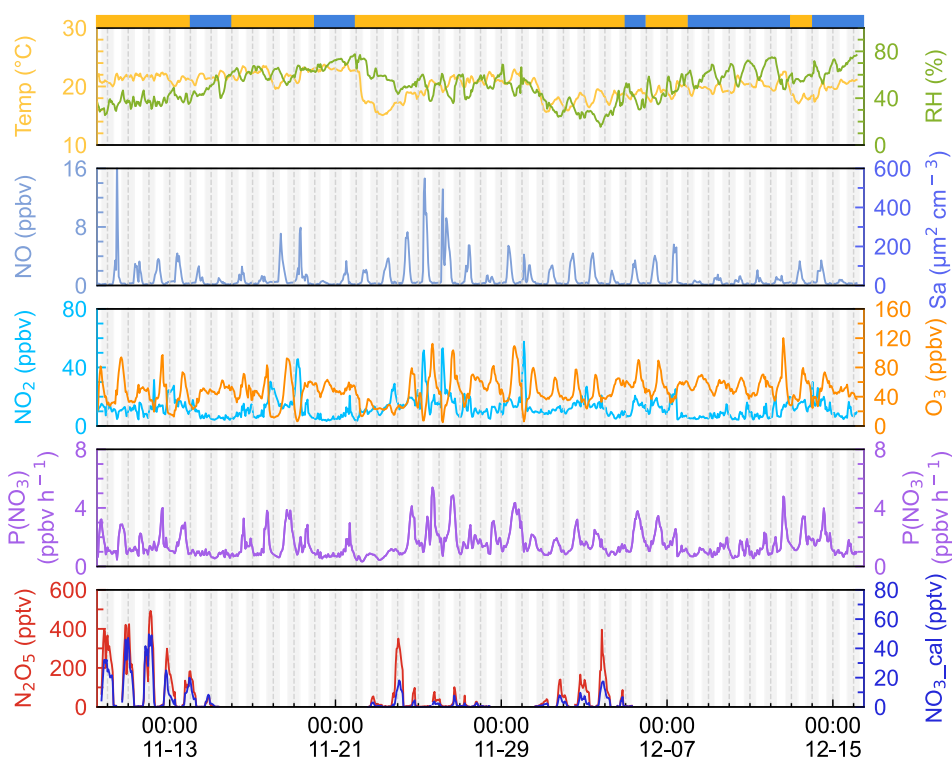
Figure 2. Time series of N_2O_5, NO_3, $P(NO_3)$, NO, NO_2, Sa, temperature, and relative
humidity in 1-hour average. NO_3 was calculated by measured N_2O_5 according to the
thermal equilibrium. The light gray shadow indicates the nighttime period. The ribbon at
the top separates the air masses into two categories, yellow for IAM and blue for CAM.

287   Ozone exhibited the characteristic of afternoon photochemical peaks especially when the
288   airmass comes from the inland. The average and maximum concentrations of ozone were
289   48.2 ± 18.2 ppbv and 120.1 ppbv, respectively. Once the maximum hourly average O_3
290   exceeded the Chinese national air quality standard (200 µg m^{-3}, equivalent to 93 ppbv), we
291   marked this day as an O_3 pollution day. There are 6 O_3 polluted days out of 37 days during
292   the campaign and all occurred during IAM periods. Meanwhile, the mixing ratio of NO,
293   NO_2, and Sa usually increased during these days, indicating that this site was strongly
294   affected by regional transport from the PRD city clusters. Previous observations by Wang
295   et al. (2018a) also found high O_3 levels in autumn on the same island due to the weak NO
296   titration and high O_3 production rate.
297   Nitrogen oxides (NO_x = NO + NO_2) were at a moderate level with an average value of 13.1
298   ± 8.2 ppbv, which is much lower than the values in PRD regions (usually > 20 ppbv, (Wang
299   et al., 2022; Yang et al., 2022; Yun et al., 2018b) and higher than those on the remote islands

300   in South China Sea (< 5 ppbv, Chuang et al., 2013). The mixing ratio of NO at nighttime
301   was low and showed small peaks during daytime. With the O_3 accumulating throughout
302   the day, NO decreased to below the instrument detection limit in the first half of the night,
303   while it began to increase as the O_3 concentration decreased in the second half of the night.
304   Given that the lifetime of NO is only a few minutes in the presence of several tens of ppbv
305   of O_3 (Dewald et al., 2022), we inferred that NO is likely originated from a local source such
306   as soil emission, boats, cooking, and so on.

307   **Table 2.** Summary of parameters on the two air mass types (mean ± standard deviation).

Species	IAM		CAM	
	All day [b]	Nighttime [b]	All day	Nighttime
O_3 (ppbv)	45.8 ± 20.2	42.9 ± 18.4	53.1 ± 11.9	51.4 ± 9.6
NO_x (ppbv)	15.1 ± 8.7	14.5 ± 9	9.2 ± 5.1	8.8 ± 4.8
NO_2 (ppbv)	13.9 ± 7.6	14.1 ± 8.3	8.6 ± 4.8	8.6 ± 4.8
NO (ppbv)	1.2 ± 2.3	0.4 ± 1.1	0.5 ± 0.6	0.2 ± 0.1
Temp (°C)	19.9 ± 2	19.9 ± 1.9	20.8 ± 1.5	20.6 ± 1.5
RH (%)	46.7 ± 12.5	47.7 ± 13.2	61.2 ± 10	64.1 ± 9.6
$P(NO_3)$ (ppbv h^{-1})	1.6 ± 0.9	1.5 ± 0.8	1.3 ± 0.8	1.2 ± 0.6
N_2O_5 (pptv)	- [c]	119.5 ± 128.6	- [c]	-
NO_3 (pptv)[a]	-	9.9 ± 12.5	-	-
$\tau_{N_2O_5}$ (min)	-	6.5 ± 6.5	-	-
τ_{NO_3} (min)	-	0.5 ± 0.7	-	-

308   Note: [a] NO_3 is calculated by the thermal equilibrium between NO_2, NO_3, and N_2O_5.
309   [b] "All day" means the 24-hour average and the "Nighttime" means the time between 18:00-
310   06:00 local time.
311   [c] Without N_2O_5 measurement in the daytime and limited N_2O_5 data during the CAM period,
312   N_2O_5, NO_3, and their lifetimes were not valid here.

313   N_2O_5 was at a moderate level on most days with a nocturnal average of 119.5 ± 128.6 pptv,
314   with high concentrations (>400 pptv in 1-hour average) in the first three days during this
315   campaign. During the nights from November 9th to 12th, the N_2O_5 concentrations were
316   significantly higher than those on other nights, with a maximum of 657.3 pptv at midnight
317   of November 12th. The NO_3 concentration (calculated based on the thermal equilibrium
318   with N_2O_5) was also moderate with an average mixing ratio of 9.9 ± 12.5 pptv, which was
319   higher than that reported on a nearby coastal site of Hong Kong Island (Yan et al., 2019).
320   Table 3 compares the N_2O_5, NO_3, and $P(NO_3)$ found in other coastal (or island) and
321   continental regions from Europe, the United States, and China. In our study, N_2O_5 and NO_3
322   were at a moderate level compared to other coastal regions when they were affected by

323   emission plumes from continental regions, such as Northwestern Europe (Morgan et al.,
324   2015), the East coast of the USA (Brown et al., 2004), and Shenzhen, China (Niu et al.,
325   2022), and were comparable with urban regions (Wang et al., 2017b; Wang et al., 2018b).
326   The concentrations of NO_3 precursors (NO_2 and O_3) at this site were much similar to some
327   rural areas, leading to a high NO_3 production rate with a daily average of 1.5 ± 0.9 ppbv h^{-1}
328   and a maximum of 5.9 ppbv h^{-1}. The average value is much higher than that reported in
329   Beijing in winter (0.4 ppbv h^{-1}, Wang et al., 2021), comparable to autumn (1.4 ± 1.7 ppbv
330   h^{-1}, Wang et al., 2017b) and even higher than that in summer Taizhou (1.01 ± 0.47 ppbv h^{-1}
331   , Wang et al., 2020a). The nocturnal average $P(NO_3)$ during this campaign was 1.4 ± 0.7
332   ppbv h^{-1}, which is higher than the average value in the warm season of China with $1.07 \pm$
333   0.38 ppbv h^{-1} (Wang et al., 2023). The high reaction rate constant for NO_2 and O_3 due to
334   the high temperature at this site is a potential explanation for the high $P(NO_3)$ values
335   observed in this study (i.e., at same NO_2 and O_3 level, if temperature increased from 10 °C
336   to 20 °C, the reaction rate constant would increase from 2.27×10^{-17} to 3.05×10^{-17}, which
337   means the $P(NO_3)$ would be 1.34 times faster). The high $P(NO_3)$ and the low concentrations
338   of N_2O_5 and NO_3 indicate intensive atmospheric oxidation capacity and fast NO_3 and N_2O_5
339   removal over the Pearl River Estuary.

340   The mean diurnal profiles of N_2O_5, together with relevant species are shown in Fig. 3.
341   Daytime N_2O_5 and NO_3 in the IAM period were shown as NaN due to the absence of
342   observation. Because of limited N_2O_5 data for the CAM period, neither N_2O_5 nor NO_3 is
343   shown in Fig. 3. NO exhibited similar diurnal variation in both periods and the mixing ratio
344   was higher in the IAM period. The wind rose plot (Fig. S1) showed high concentrations of
345   NO originating from the north characterized by the outflow from PRD regions. However,
346   NO_2 differed in the two periods, showing high anti-correlation with O_3 only in the IAM
347   period and little diurnal variation in the CAM period.
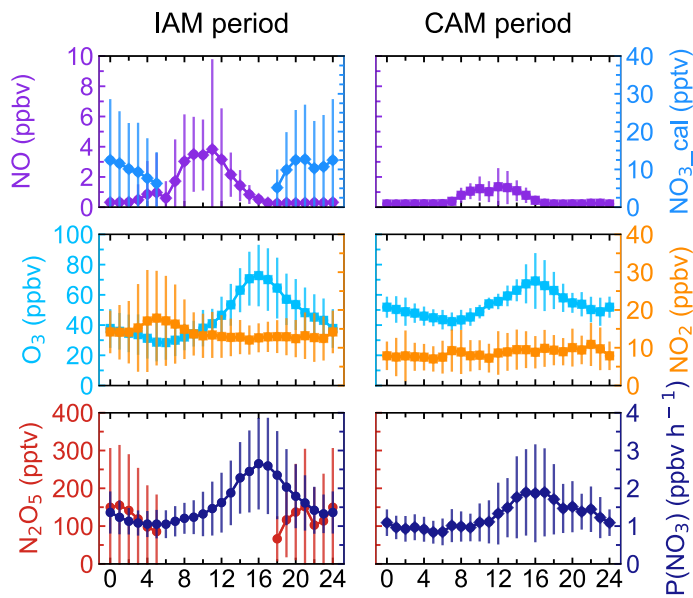
Figure 3. Mean diurnal profiles of N_2O_5, NO_3, $P(NO_3)$, and relevant parameters in the two types of air masses. NO_3 was calculated from N_2O_5. Neither N_2O_5 nor NO_3 was shown during CAM period because of limited N_2O_5 measurement.

Ozone exhibited a typical diurnal pattern for all air masses, gradually increasing until its peak at 16:00 and then slowly decreasing throughout the night until its lowest mixing ratio was reached at about 06:00. Compared to the CAM period, the lower minimum hourly O_3 concentration and a small peak of NO_2 in the early morning indicated that NO titration effect was stronger in the IAM period, and the higher maximum of O_3 concentration in IAM indicated that photochemical formation of O_3 and/or transport was faster to completely offset the titration. In addition, the higher NO_x and VOC concentrations (as shown in Table S1) in the IAM period facilitated O_3 formation. With the elevated precursor concentrations (NO_2 and O_3) in the IAM period, N_2O_5 and NO_3 accumulated rapidly after sunset, reaching their peak values (492.1 pptv and 49.6 pptv for each). $P(NO_3)$ was highly consistent with O_3 in diurnal variation and reached the peak at 16:00, with peak values of 2.7 ppbv h^{-1} (IAM) and 1.9 ppbv h^{-1} (CAM), as well as a nocturnal average value of 1.5 ± 0.8 ppbv h^{-1} (IAM) and 1.2 ± 0.6 ppbv h^{-1} (CAM), respectively. The $P(NO_3)$ of CAM was consistent with the observation when the air mass over eastern Shenzhen was transported from the clean area or sea surface (1.2 ± 0.3 ppbv h^{-1}, Niu et al., 2022).

Table 3. Summary of field-observed N_2O_5, NO_2, O_3 concentrations, and NO_3 production rate.

Region	Location	Time	N_2O_5 (pptv)	NO_3 (pptv)	NO_2 (ppbv)	O_3 (ppbv)	P (NO_3) (ppbv hr^{-1})	References
Urban	Jinan, China	Aug.-Sep.,2014	22 ± 13 (max 278)	16±9 (max 95)	74.6	55	/	(Wang et al., 2017c)
Urban	Shanghai, China	Aug.-Oct., 2011	310 ± 380		0-76	23 ± 8 (max 57)	1.10 ±1.09	(Wang et al., 2013)
Urban	Beijing, China	May-Jul., 2016	100–500 (max 937)	27	/	/	1.2 ± 0.9	(Wang et al., 2018b)
Urban	Mt. Tai, China	Jul.-Aug.,2014	6.8±7.7	/	16.4 (±6.1)	88.6 (±16.6)	0.45±0.40	(Wang et al., 2017d)
Urban	Heshan, China	Sep.-Nov., 2019	64 ± 145 (night) (max 1180)	max 90	21.0±10.4	75.2±20.9 (max 152.8)	2.5 ± 2.1 (day) 1.8 ±1.5 (night)	(Wang et al., 2022)
Urban	Beijing, China	Sep.-Oct., 2019	68.0 ±136.7	/	35.1 ±16.6	27.7 ±25.2	2.25 ±2.02	(Wang et al., 2017b)
Suburban	Changzhou, China	May-Jul., 2019	53.4 ± 66.1 (max 304.7)	4.7 ± 3.5 (max 17.7)	13.7 ± 8.9	48.4 ± 27.8	1.7 ± 1.2 (max 7.7)	(Lin et al., 2022)
Rural	Wangdu, China	Jun.-Jul., 2014	<200 (max 430)	/	10-80	(max 146)	1.7 ±0.6	(Tham et al., 2016)
Rural	Taizhou, China	May-Jul., 2018	26.0 ± 35.7 (max 492)	4.4 ± 2.2 (max 150)	28.28 ± 18.57	48.2 ± 32.5	1.01 ± 0.47 (night)	(Wang et al., 2020a)
Coastal	Tai Mo Shan, HK	Nov.-Dec., 2013	0.5-11.8 ppbv	-	7.88	68.5	0.01-2	(Brown et al., 2016)
Coastal	East coast of USA	Jun.-Aug., 2002	85	17	6	35	/	(Brown et al., 2004)
Coastal	California, USA	Jan.,2004	0-200	/	0-15	15-35		(Wood et al., 2005)
Coastal	Southern Spanish	Nov.-Dec.,2018	~500 (max)	/	1-15	15-40		(Crowley et al., 2011)
Coastal	Shenzhen, China	Sep.-Oct., 2019	55.6 ± 89 (max 1420) 45.4 ± 55.2 (BAM)	/	6.2	88.9±24.6	2.9 ± 0.5 (UAM) 1.2 ± 0.3 (BAM)	(Niu et al., 2022)
Coastal	Northwestern Europe	Jul., 2010	670	/	0.5–2	30–40	/	(Morgan et al., 2015)
Island	Hok Tsui, HK	Aug.-Sep., 2012	17±33 (max 336)	7 ± 12	6 ± 7	33 ± 24	/	(Yan et al., 2019)
Island	Wanshan, China	Nov.-Dec. 2021	107.22 ± 125.17	7.56 ± 10.95	13.14 ± 8.68	43.75 ± 18.49	1.38 ±0.83	This work

Notes: UAM means air masses coming from continental areas, and BAM means air masses coming from background marine areas. Mean values are in the form of mean ± standard deviation or single data. The maximum was noted in the table.

3.2 The lifetimes of N₂O₅ and NO₃

Steady-state lifetime is one of the most common and useful diagnostics for NO_3 and N_2O_5 analysis in the atmosphere (Brown et al., 2003; Wang et al., 2018b; Wang et al., 2020a; Brown et al., 2016). As shown in Fig. 4, τ_{NO_3} was low during the whole campaign with an average of 0.5 ± 0.7 min. $\tau_{N_2O_5}$ showed a similar pattern to τ_{NO_3} but had a much higher value, ranging from 0 to 34.1 min with an average of 6.1 ± 6.5 min. The N_2O_5 lifetime was higher in the first half of the campaign (11.5 min, November 9th to 14th) than in the second half (3.5 min, November 22th to 28th). The difference was mainly due to the N_2O_5 mixing ratio rather than P(NO₃), as P(NO₃) shows no significant difference during the whole observation (Fig. 2).
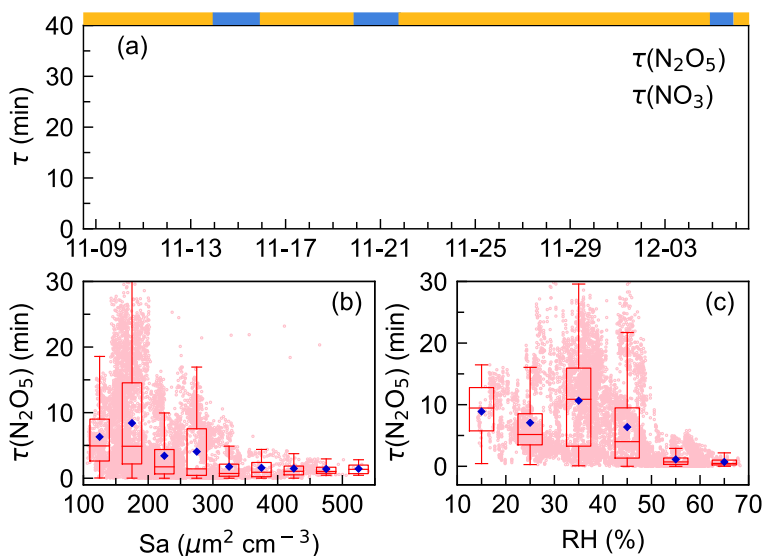
Figure 4. Time series of N₂O₅ and NO₃ lifetimes (a) and variations of nocturnal N₂O₅ lifetime as a function of aerosol surface area density, Sa (b), and relative humidity, RH (c). The blue diamond represents the average $\tau_{N_2O_5}$ and pink dots represent the scatter data point in 1 min. The ribbon at the top separates the air masses into two categories, yellow for IAM and blue for CAM.

$\tau_{N_2O_5}$ values were comparable to those measured on the coastline of Finokalia, Greece for a median of 5 min (Vrekoussis et al., 2004; Vrekoussis et al., 2007), but much lower than those previously reported in the residual layer in Hong Kong for 1-5 h (Brown et al., 2016). In comparison, the lifetimes were much longer than in inland urban areas, for example, 0.93 ± 1.13 min in Taizhou (Li et al., 2020), 1.6 ± 1.5 min in Changzhou (Lin et al., 2022) for YRD regions, 1.1-10.7 min (Zhou et al., 2018) and 4.5 ± 4.0 min (Wang et al., 2018b) in Beijing. Typically, high aerosol loading, more intensive VOC, and NO emissions in these

393   areas led to enhanced N_2O_5 uptake and reactions of NO_3 with VOC. While in this site,
394   measurement indicated that the peak diameter in the particle number distribution was small
395   during the whole campaign and indicated no significant difference between two air masses
396   with respect to the aerosol diameters (Fig. S2). S_a value ranged from 29 μm^2 cm^{-3} to 557
397   μm^2 cm^{-3}. All of these indicated the atmosphere was relatively clean (Wang et al., 2017b),
398   making N_2O_5 uptake slow. Fig. 4b shows N_2O_5 lifetime decreased rapidly from 8.3 min to
399   1.7 min when S_a increased up to 300 μm^2 cm^{-3} and then remained at relatively low constant
400   levels though S_a still increased. Such a trend of $\tau_{N_2O_5}$-S_a dependence was consistent with
401   previous observations and varied in exact values (Zhou et al., 2018; Wang et al., 2018b; Li
402   et al., 2020). Fig. 4c. showed that $\tau_{N_2O_5}$ decreased as RH increased ($>40\%$) possibly due
403   to the hygroscopic aerosol growth and the dependence of the N_2O_5 uptake coefficient on
404   the RH (Brown and Stutz, 2012). Overall, the trend is consistent with previous works, while
405   the large discrepancy of the dependence implied that N_2O_5 uptake was not the dominant
406   NO_3 loss process.

407   ## 3.3 The NO_3 reactivity and N_2O_5 uptake coefficients

408   The concurrent high $P(NO_3)$ and low NO_3 lifetime imply high NO_3 reactivity as well as a
409   large nocturnal NO_3 loss process at DWS. The NO_3 reactivity towards VOCs was
410   calculated by Eq. 4, towards which were categorized into anthropogenic VOC and biogenic
411   VOC (Gu et al., 2021). Throughout the campaign, $k(NO_3)$ varied considerably (Fig. 5a),
412   showing relatively high and fluctuated values when the airmasses featured IAM. The
413    $k(NO_3)$ ranged from 1.6×10^{-3} s^{-1} to 2.4×10^{-2} s^{-1} with the daily average of $4.6 \pm 2.8 \times 10^{-3}$
414   s^{-1}. Low values of $k(NO_3)$ were observed from December 9th to 12th when the air masses
415   originate from coastal or offshore from the east and southeast, which features the outflow
416   of coastal cities like Hong Kong and Shenzhen.

417   Fig. 5b shows the mean diurnal profile of $k(NO_3)$, where a trend of high values in the
418   daytime and low values at nighttime are observed. Anthropogenic VOC, especially cresol,
419   dominated the daily trend of $k(NO_3)$, while biogenic VOC-$k(NO_3)$ showed no significant
420   diurnal variation. Except cresol, other highly reactive VOC showed little change
421   throughout the day. Regarding the biogenic VOC-$k(NO_3)$, the concentrations of
422   monoterpene, isoprene, and DMS changed smoothly although their emissions would
423   increase with elevated temperature and sunlight during daytime (Fuentes. et al., 2000). The
424   detailed contributions of VOC categories to $k(NO_3)$ were shown in Fig. 5c. The $k(NO_3)$
425   was $5.6 \pm 2.8 \times 10^{-3}$ s^{-1} and $3.7 \pm 2.5 \times 10^{-3}$ s^{-1} on average for daytime and nighttime,
426   respectively. The daytime distribution of $k(NO_3)$ differed from that at the mountaintop of
427   Tai Mo Shan in Hong Kong (Brown et al., 2016). During the nighttime, anthropogenic
428   VOC-$k(NO_3)$ tripled the biogenic VOC-$k(NO_3)$ and was dominated by cresol (26.4%). The

nighttime $k(NO_3)$ corresponded to a NO_3 lifetime of 4.5 min, which was about 10 times the
lifetime derived from steady-state analysis, indicating that the reaction of NO_3 with VOC
was not significant enough. The faster NO_3 loss rate also indicated the less aged air mass
that was influenced by surface-level emissions.
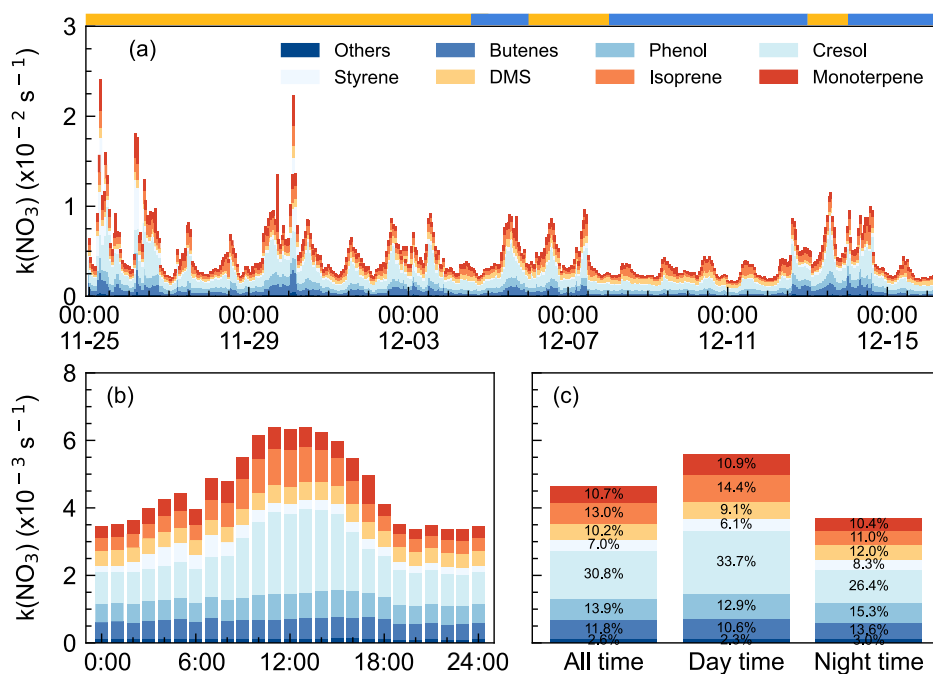
Figure 5. NO_3 reactivity via VOCs during the campaign. (a) $k(NO_3)$ time series from Nov.
25th to Dec. 15th; (b) mean diurnal profiles; and (c) the relative contribution in different
categories. The ribbon at the top separates the air masses into two air masses types, yellow
for IAM and blue for CAM.

We showed that NO_3 reactivity and its composition in this study exhibited significant
differences compared to other urban or forested regions (Wang et al., 2017d; Ayres et al.,
2015; Brown et al., 2016; Lin et al., 2022). Although anthropogenic VOCs played a
dominant role, accounting for 66.1%, the major contributors were not low-carbon alkenes
but phenol (13.9%, $0.64 \pm 0.28 \times 10^{-3}$ s^{-1}) and cresol (30.8%, $1.4 \pm 1.0 \times 10^{-3}$ s^{-1}), which
have received little attention in previous studies. Despite their relatively low concentrations,
averaging 7 ± 3 pptv and 4 ± 3 pptv respectively, their substantial contribution to $k(NO_3)$
is notable due to their fast rate constants (3.8×10^{-12} cm^3 molecule^{-1} s^{-2} and 1.4×10^{-11} cm^3
molecule^{-1} s^{-2} at 298 K, respectively) for reaction with NO_3. Considering that the measured
phenol and cresol concentration is low and near the instrumental detection limit, we note
this may bring some uncertainties in quantifying the contribution to the total NO_3 reactivity
and NO_3 loss rate. These substances are mainly secondary species from aromatic

17

450 compounds and higher concentrations have also been observed, such as in the Strasbourg
451 area, France (14 pptv, Delhomme et al., 2010) and in Great Dun Fell, UK (16 pptv, Lüttke
452 et al., 1997). Hence, these phenolic compounds were potentially important but often
453 overlooked for their contributions to NO_3 reactivity in urban areas, and their reactions with
454 NO_3 may also contribute to the formation of nitrophenol. These reactions warrant further
455 attention in future research. Regarding biogenic VOCs, besides the contributors commonly
456 observed in forest regions such as monoterpenes and isoprene, the marine emissions
457 indicator, dimethyl sulfide (DMS), contributed 10.2% to NO_3 reactivity (daily average).
458 Previous studies have suggested that DMS may serve as a major direct sink for NO_3 in
459 clean marine regions (Allan et al., 1999; Aldener et al., 2006; Brown et al., 2007). However,
460 this study reveals that anthropogenic VOC emissions significantly enhanced the NO_3
461 reactivity in marine areas, highlighting the crucial influence of anthropogenic activities on
462 marine atmospheric chemistry.

463 As shown in Fig. 6a, $k(NO_3)$ differed significantly between the inland and coastal air
464 masses, with $5.2 \pm 3.1 \times 10^{-3}$ s^{-1} and $3.7 \pm 1.9 \times 10^{-3}$ s^{-1} on average in IAM and CAM periods,
465 respectively. Of which anthropogenic VOC-$k(NO_3)$ in IAM ($3.5 \pm 2.3 \times 10^{-3}$ s^{-1}) was higher
466 than in CAM ($2.3 \pm 1.4 \times 10^{-3}$ s^{-1}) and dominant in both air masses, while biogenic VOC-
467 $k(NO_3)$ was comparable ($1.7 \pm 0.9 \times 10^{-3}$ s^{-1} and $1.4 \pm 0.6 \times 10^{-3}$ s^{-1} for IAM and CAM,
468 respectively). The difference indicated that this region was affected by long-range transport
469 emissions to a certain extent. The pie charts in Fig. 6b showed different VOC categories
470 that contributed to $k(NO_3)$ in two periods with AVOC dominant at any time. The change in
471 the relative contribution of various VOCs to $k(NO_3)$ varied simultaneously throughout the
472 day, showing an increase in butene, phenol, and DMS, and a decrease in cresol and
473 monoterpene from daytime to nighttime.

474 N_2O_5 heterogeneous uptake on aerosol is one of the vital loss processes of NO_3 and the
475 uptake coefficient varied greatly under different environmental conditions. For instance,
476 $\gamma(N_2O_5)$ can reach up to 0.072 in polluted urban regions (Wang et al., 2017b; Wang et al.,
477 2018b; Lu et al., 2022; Li et al., 2020), while usually below 0.03 in coastal areas (Brown
478 et al., 2016; Morgan et al., 2015; Niu et al., 2022). N_2O_5 uptake coefficient can be gotten
479 from the pseudo steady state method by assuming that N_2O_5 and NO_3 have achieved a
480 steady state (Brown et al., 2009), in which the fitted slope represents $\gamma(N_2O_5)$ and the
481 intercept represents the direct loss rate coefficient, $k(NO_3)$ (as shown in Eq. 8). However,
482 this approach failed to generate valid results in our study since a negative slope or intercept
483 was observed (Fig. S4). These results indicated that a large NO_3 removal process existed
484 at this site, making it unable to approach a stable state. The $\gamma(N_2O_5)$ was also calculated
485 from Nov. 9th to 16th by using the simplified parameterization, as shown in Eq. 9. The
486 parameterized average $\gamma(N_2O_5)$ showed a large variation ranging from 0.0014 to 0.0299,

487 with an average of 0.0095 ± 0.0059. This value is within the range from <0.0016 to 0.03
488 derived from the ambient observation around other coastal areas (Niu et al., 2022; Yun et
489 al., 2018a; Brown et al., 2006; Brown et al., 2016; Morgan et al., 2015) and smaller than
490 the polluted North China Plain (Wang et al., 2017c; Wang et al., 2017b; Wang et al., 2017d;
491 Tham et al., 2018).

492
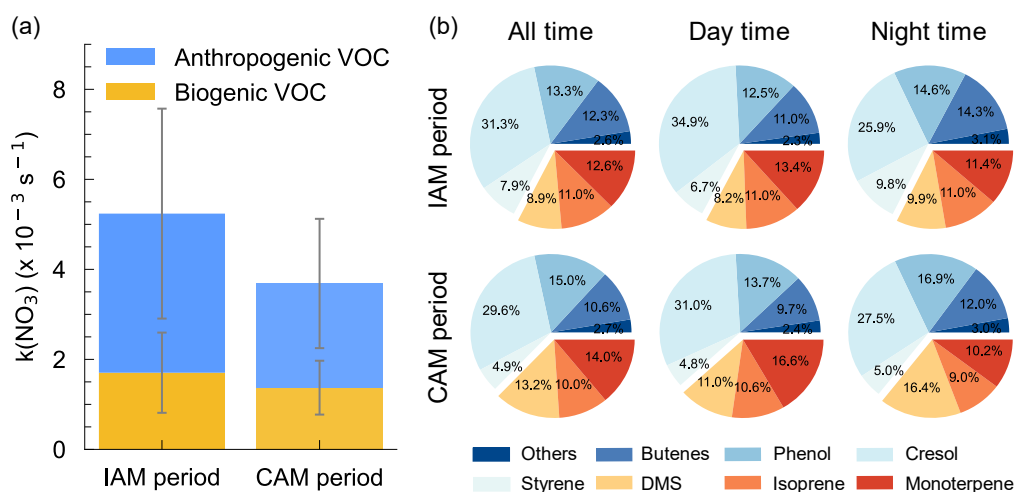
Figure 6. (a) Distributions of $k(NO_3)$ from AVOC and BVOC for both IAM and CAM
period. The error bar indicates the standard deviation. (b) The relative contribution of VOC
categories to the $k(NO_3)$.

3.4 The NO_3 loss budget

To assess the contribution of various loss processes to the total NO_3 removal, we calculated
their loss rate and the loss ratio, $LR(NO_3)$. The $LR(NO_3)$ is defined as the sum of the loss
rate by process X (VOC or N_2O_5 uptake) to the total NO_3 loss rate, here the total NO_3 loss
rate is represented by $P(NO_3)$ since we cannot quantify the total NO_3 loss rate due to the
NO concentration below the limit of instrument detection. Due to the data absence of
measured VOCs or N_2O_5 during certain periods, the loss proportion of VOCs and N_2O_5
uptake in NO_3 loss only presented from Nov. 26th to Dec. 5th during which all air masses
originated from continental China. As shown in Fig. 7, a closer examination revealed that
the nights can be divided into two periods, period I: November 25th to 28th when the loss
ratio of VOC and N_2O_5 uptake remained below 3%, and period II: November 30 to
December 4 when the loss ratio was higher. Both periods had large nocturnal NO_3
production rates with an average of 2.1 ± 1.1 ppbv h^{-1} in period I and 1.4 ± 0.6 ppbv h^{-1} in
period II, respectively.

510   N_2O_5 uptake rate was larger in period I (0.01 ± 0.01 ppbv h^{-1}) than that in period II (0.006
511   ± 0.004 ppbv h^{-1}), which can be explained by the increased RH, Sa, and N_2O_5 concentration
512   as shown in Fig. 2. The loss ratio of these processes was shown in Fig. 7b, the total NO_3
513   loss through reactions with VOCs and N_2O_5 uptake accounted for less than 20%, with an
514   average of 1.2% (period I) and 5.3% (period II), respectively. This result shows that the
515   nighttime NO_3 chemistry may be almost negligible to the NOx removal compared with the
516   day OH + NO_2 pathway according to previous works reported in urban regions (Wang et
517   al., 2017b; Wang et al., 2020a). The diurnal variation of the NO_3 loss fraction of both
518   periods was shown in Fig. 7c and 7d, revealing that NO_3 loss via N_2O_5 uptake and VOCs
519   was slightly higher in the early evening and relatively stable in the late evening. The pie
520   charts in the center were the relative contribution between VOCs and N_2O_5 uptake, showing
521   that VOCs were overwhelming compared with N_2O_5 uptake during the two periods, with
522   an average of 68.4% and 91.7% during the first and second periods, respectively.

523   To better understand the nocturnal oxidation of VOCs, we compared the nighttime
524   oxidation of VOCs by NO_3 with O_3. Since OH was not measured and OH is often regarded
525   as a vital daytime oxidant (Finlayson-Pitts, 2000; Lu et al., 2010), we did not consider OH
526   oxidation in the nighttime. Figure S4 showed the diurnal pattern of VOC loss rate by NO_3
527   and O_3, NO_3 predominantly achieves its peak oxidation rates (0.07 ppbv h^{-1}) during the
528   initial half of the night, accounting for 63.1% of the total VOC oxidation on nocturnal
529   average. Meanwhile, O_3 also makes a contribution to VOC oxidation, mainly owing to its
530   relatively high nighttime concentration levels (42.9 ± 18.4 ppbv).
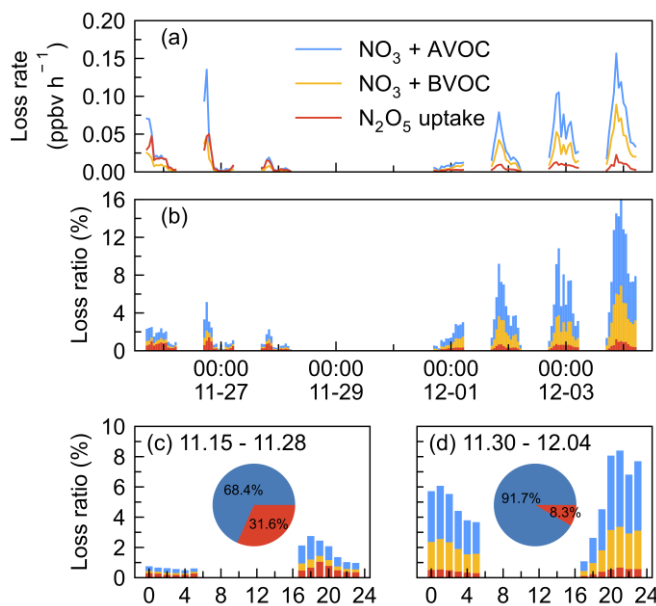
531

532   **Figure 7.** Time series of (a) the loss rate of NO_3 reactions with AVOC, BVOC, and N_2O_5

533   uptake, and (b) fractional contribution to the NO_3 loss during the nighttime by taking

534    $P(NO_3)$ as the total NO_3 loss in the IAM period. The mean diurnal profiles of NO_3 loss

535   ratio in two periods (c) November 25th - 28th, and (d) November 30th - December 4th. Pie

536   charts in the center showed the relative contribution of VOCs (blue) and N_2O_5 uptake (red)

537   in NO_3 loss.

538   Due to the difficulty in experimental quantifying $\gamma(N_2O_5)$, the estimation of N_2O_5 uptake

539   in NO_3 loss may include some uncertainty. Considering the uncertainty both in

540   parameterized $\gamma(N_2O_5)$ and the NO_3 reactivity calculation, three sensitivity tests were

541   conducted to assess the uncertainty in period II because of the relatively high loss ratio in

542   the above analysis (Fig. 8), and the three cases were used to represent the upper limit of

543   their contribution to NO_3 loss. Case 1 represents the overrated contribution of N_2O_5 uptake

544   by taking $\gamma(N_2O_5) = 0.08$, which was the high value reported in high N_2O_5 and $ClNO_2$

545   plume of Shenzhen (Niu et al., 2022) and approximately seven times the parameterized

546   value at this site. In this case, the fraction of NO_3+VOCs and N_2O_5 uptake was significantly

547   elevated to account for approximately 30% of NO_3 loss. Case 2 shows the total NO_3

548   reactivity reached an average of 5.0×10^{-3} s^{-1} by taking β-pinene as the total monoterpene

549   because of the higher reaction rate constant. The weak change in the loss ratio indicates the

550   reactions of NO_3 with VOC may not be sensitive to the weights of monoterpenes, since the

551   contribution of monoterpenes to the NO_3 reactivity is not dominant. Case 3 is the synthesis

552   of Case 1 and Case 2 by considering higher N_2O_5 uptake coefficient and higher $k(NO_3)$ to

553   represent the upper limit of N_2O_5 uptake and NO_3 reaction with VOCs to NO_3 loss, whose

554   result is slightly higher than the contribution of Case 1. Nevertheless, the quantified upper

555   contribution was still less than half. Thus, we conclude that most of the NO_3 loss was not

556   well accounted for even considering the uncertainties.
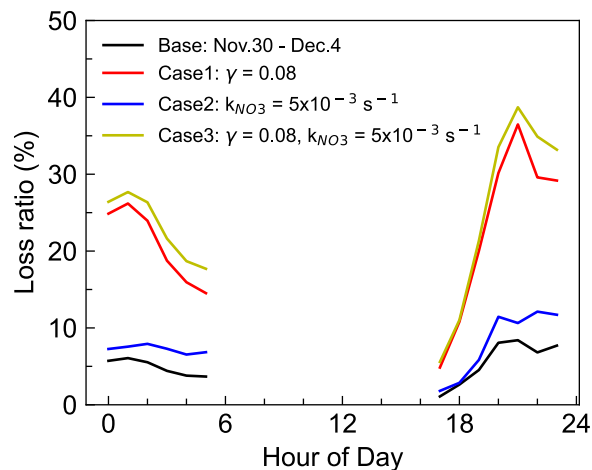
557

558   **Figure 8.** Three sensitivity tests for the contribution of VOCs and N_2O_5 uptake to the NO_3

loss during the nighttime of period II (November 30th - December 4th). Case 1 takes γ(N$_2$O$_5$) = 0.08, which is the high value reported in the previous study. Case 2 takes β-pinene as the total monoterpene with a higher reaction rate constant, and Case 3 is the synthesis of the above two cases to represent the upper limit of the contribution.

The NO$_3$ reaction with NO was often considered to be one of the dominant loss processes during the daytime since at nighttime NO decreased to low levels, thus not considered in the above analysis. However, by taking NO into consideration although at low concentration levels below the detection limit of the instrument (0.4 ppbv), the contribution of NO to the nighttime NO$_3$ loss exceeded 100% frequently as shown in Fig. S5. Due to the rapid reaction between NO and NO$_3$, several pptv concentrations of NO could effectively account for most NO$_3$ loss in a relatively clean coastal environment (Crowley et al., 2011). Nevertheless, limited by NO precise measurement, we considered the following assessments to understand the total NO$_3$ loss processes (Fig. 9). By assuming NO at a constant value of 40-400 pptv, more than 80% of the total NO$_3$ loss can be well explained. Although some loss remained unidentified, these results underline that NO, often considered to be important during daytime, was the predominant NO$_3$ loss way during nighttime at this study site. This also suggests accurate measurement of low NO concentrations is crucial for identifying removal pathways of nocturnal NO$_3$ oxidants and has significant implications for nighttime atmospheric chemistry. We can infer that the nocturnal chemical NO$_3$ reactions would be largely enhanced once without NO emission in the open ocean after the air mass passes through this site, indicating the strong influences of the urban outflow to the downwind marine areas with respect to nighttime chemistry.
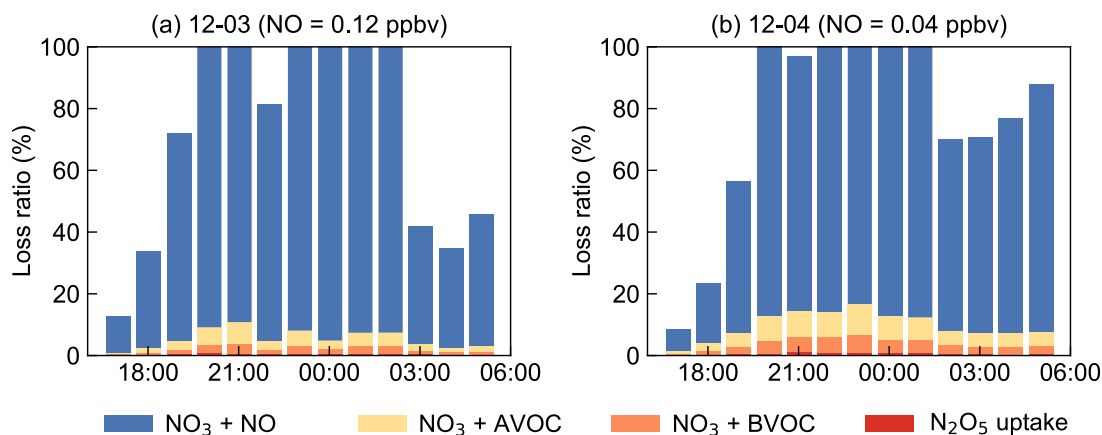
Figure 9. Examples for the assessment of NO$_3$ loss process by assuming NO as constant values to approximately explain about 80% of the budget.

584 For the absence of measured N_2O_5 during the CAM period, we compared the $k(NO_3)$ and
585 the reactivity of N_2O_5 uptake ($k_{het}K_{eq}NO_2$) to indirectly reflect NO_3 removal process.
586 Overall, the NO_3 reactivity values from VOCs and N_2O_5 uptake during nighttime was
587 relatively comparable, for 56.5% and 43.5%, respectively. This indicates that VOCs still
588 had a slightly larger contribution than N_2O_5 uptake during the CAM period, which is
589 consistent with the findings in southern China (Brown et al., 2016) and on the east coast of
590 the USA (Aldener et al., 2006).

591 **4. Summary and Conclusion**

592 This study presents the first observation of nocturnal nitrogen oxide species, N_2O_5, at a
593 typical marine site (Da Wan Shan Island, Zhuhai) in the north of the South China Sea during
594 the winter of 2021. Although Da Wan Shan Island was almost free of local anthropogenic
595 emissions, the air pollutants from the megacities of the Pearl River Delta were transported
596 to this area by northerly or northeasterly winds during the measurement period. The
597 maximum ratio of N_2O_5 was 657.27 pptv (1 min average) and the nocturnal average was
598 119.5 ± 128.6 pptv. The NO_3 production rate was comparable to that in urban areas such as
599 north China and the Yangtze River Delta, with an average value of 1.5 ± 0.9 ppbv h^{-1} and
600 a maximum of up to 5.84 ppbv h^{-1}, indicating an active nighttime chemical process in that
601 area.

602 Further analysis of N_2O_5 and NO_3 steady state lifetimes indicates that NO_3 had a very short
603 average life of 0.5 ± 0.6 minutes, which was to some extent comparable to that in urban
604 areas in summer. The combination of the high NO_3 production rate and short lifetime
605 suggests a rapid NO_3 loss at night. While N_2O_5 uptake is inefficient in relatively clean air
606 masses. The nighttime $k(NO_3)$ corresponded to a NO_3 lifetime of 4.5 minutes, indicating
607 that VOCs also contribute little to NO_3 loss. Both VOC and N_2O_5 uptake can only explain
608 less than 20% of the total loss. The fast NO_3 loss rate also indicated the air mass that was
609 influenced by local surface-level emissions. We infer that the local weak NO emission may
610 significantly change the near-surface chemical pattern of NO_3 chemistry, which may result
611 in a huge difference between the observed results on the island and those on the sea surface.
612 We suggested that future field measurements should be made on sea surfaces away from
613 islands, such as ship-based cruise observation, to get a comprehensive understanding of the
614 nocturnal NO_3 chemistry in the background marine regions.

615

Appendix A Supplementary data
Supplementary data associated with this article can be found in the online version at xxxxxx.

Reference

Aldener, M., Brown, S. S., Stark, H., Williams, E. J., Lerner, B. M., Kuster, W. C., Goldan, P. D., Quinn, P. K., Bates, T. S., Fehsenfeld, F. C., and Ravishankara, A. R.: Reactivity and loss mechanisms of NO_3 and N_2O_5 in a polluted marine environment: Results from in situ measurements during New England Air Quality Study 2002, Journal of Geophysical Research-Atmospheres, 111, Artn D23s73, Doi 10.1029/2006jd007252, 2006.

Allan, B. J., Carslaw, N., Coe, H., Burgess, R. A., and Plane, J. M. C.: Observations of the nitrate radical in the marine boundary layer, Journal of Atmospheric Chemistry, 33, 129-154, Doi 10.1023/A:1005917203307, 1999.

Atkinson, R., Baulch, D. L., Cox, R. A., Crowley, J. N., Hampson, R. F., Hynes, R. G., Jenkin, M. E., Rossi, M. J., and Troe, J.: Evaluated kinetic and photochemical data for atmospheric chemistry: Volume I - gas phase reactions of O_x, HO_x, NO_x and SO_x species, Atmospheric Chemistry and Physics, 4, 1461-1738, DOI 10.5194/acp-4-1461-2004, 2004.

Ayres, B. R., Allen, H. M., Draper, D. C., Brown, S. S., Wild, R. J., Jimenez, J. L., Day, D. A., Campuzano-Jost, P., Hu, W., de Gouw, J., Koss, A., Cohen, R. C., Duffey, K. C., Romer, P., Baumann, K., Edgerton, E., Takahama, S., Thornton, J. A., Lee, B. H., Lopez-Hilfiker, F. D., Mohr, C., Wennberg, P. O., Nguyen, T. B., Teng, A., Goldstein, A. H., Olson, K., and Fry, J. L.: Organic nitrate aerosol formation via NO_3 + biogenic volatile organic compounds in the southeastern United States, Atmospheric Chemistry

657   and Physics, 15, 13377-13392, 10.5194/acp-15-13377-2015, 2015.

658   Behnke, W., and, V., Scheer, and, C., and Zetzsch: 16 O 04 Formation of $ClNO_2$ and HNO_3

659   in the presence of N_2O_5 and wet pure NaCl- and wet mixed $NaCl/Na_2SO_4$- aerosol, J

660   Aerosol Sci, 24, S115-S116, 1993.

661   Bertram, T. H. and Thornton, J. A.: Toward a general parameterization of N_2O_5 reactivity

662   on aqueous particles: the competing effects of particle liquid water, nitrate and

663   chloride, Atmospheric Chemistry and Physics, 9, 8351-8363, 2009.

664   Brown, S. S. and Stutz, J.: Nighttime radical observations and chemistry, Chem Soc Rev,

665   41, 6405-6447, Doi 10.1039/C2cs35181a, 2012.

666   Brown, S. S., Stark, H., and Ravishankara, A. R.: Applicability of the steady state

667   approximation to the interpretation of atmospheric observations of NO_3 and N_2O_5,

668   Journal of Geophysical Research-Atmospheres, 108, Artn 4539, Doi

669   10.1029/2003jd003407, 2003.

670   Brown, S. S., Dube, W. P., Tham, Y. J., Zha, Q. Z., Xue, L. K., Poon, S., Wang, Z., Blake,

671   D. R., Tsui, W., Parrish, D. D., and Wang, T.: Nighttime chemistry at a high altitude

672   site above Hong Kong, Journal of Geophysical Research-Atmospheres, 121, 2457-

673   2475, 10.1002/2015jd024566, 2016.

674   Brown, S. S., Ryerson, T. B., Wollny, A. G., Brock, C. A., Peltier, R., Sullivan, A. P., Weber,

675   R. J., Dube, W. P., Trainer, M., Meagher, J. F., Fehsenfeld, F. C., and Ravishankara, A.

676   R.: Variability in nocturnal nitrogen oxide processing and its role in regional air quality,

677   Science, 311, 67-70, DOI 10.1126/science.1120120, 2006.

678   Brown, S. S., Dube, W. P., Peischl, J., Ryerson, T. B., Atlas, E., Warneke, C., de Gouw, J.

679   A., Hekkert, S. T., Brock, C. A., Flocke, F., Trainer, M., Parrish, D. D., Feshenfeld, F.

680   C., and Ravishankara, A. R.: Budgets for nocturnal VOC oxidation by nitrate radicals

681   aloft during the 2006 Texas Air Quality Study, Journal of Geophysical Research-

682   Atmospheres, 116, Artn D24305, 10.1029/2011jd016544, 2011.

683   Brown, S. S., Dube, W. P., Fuchs, H., Ryerson, T. B., Wollny, A. G., Brock, C. A., Bahreini,

684   R., Middlebrook, A. M., Neuman, J. A., Atlas, E., Roberts, J. M., Osthoff, H. D.,

685   Trainer, M., Fehsenfeld, F. C., and Ravishankara, A. R.: Reactive uptake coefficients

686   for N2O5 determined from aircraft measurements during the Second Texas Air

687   Quality Study: Comparison to current model parameterizations, Journal of

688   Geophysical Research-Atmospheres, 114, Artn D00f10, 10.1029/2008jd011679, 2009.

689   Brown, S. S., Dube, W. P., Osthoff, H. D., Stutz, J., Ryerson, T. B., Wollny, A. G., Brock,

690   C. A., Warneke, C., De Gouw, J. A., Atlas, E., Neuman, J. A., Holloway, J. S., Lerner,

691   B. M., Williams, E. J., Kuster, W. C., Goldan, P. D., Angevine, W. M., Trainer, M.,

692   Fehsenfeld, F. C., and Ravishankara, A. R.: Vertical profiles in NO_3 and N_2O_5

693   measured from an aircraft: Results from the NOAA P-3 and surface platforms during

694   the New England Air Quality Study 2004, Journal of Geophysical Research-

695   Atmospheres, 112, Artn D22304, 10.1029/2007jd008883, 2007.

Brown, S. S., Dibb, J. E., Stark, H., Aldener, M., Vozella, M., Whitlow, S., Williams, E. J., Lerner, B. M., Jakoubek, R., Middlebrook, A. M., DeGouw, J. A., Warneke, C., Goldan, P. D., Kuster, W. C., Angevine, W. M., Sueper, D. T., Quinn, P. K., Bates, T. S., Meagher, J. F., Fehsenfeld, F. C., and Ravishankara, A. R.: Nighttime removal of NOx in the summer marine boundary layer, Geophysical Research Letters, 31, Artn L07108, Doi 10.1029/2004gl019412, 2004.

Chen, X., Wang, H., and Lu, K.: Interpretation of NO_3–N_2O_5 observation via steady state in high-aerosol air mass: the impact of equilibrium coefficient in ambient conditions, Atmospheric Chemistry and Physics, 22, 3525-3533, 10.5194/acp-22-3525-2022, 2022.

Chuang, M.-T., Chang, S.-C., Lin, N.-H., Wang, J.-L., Sheu, G.-R., Chang, Y.-J., and Lee, C.-T.: Aerosol chemical properties and related pollutants measured in Dongsha Island in the northern South China Sea during 7-SEAS/Dongsha Experiment, Atmospheric Environment, 78, 82-92, 10.1016/j.atmosenv.2012.05.014, 2013.

Crowley, J. N., Thieser, J., Tang, M. J., Schuster, G., Bozem, H., Beygi, Z. H., Fischer, H., Diesch, J. M., Drewnick, F., Borrmann, S., Song, W., Yassaa, N., Williams, J., Pohler, D., Platt, U., and Lelieveld, J.: Variable lifetimes and loss mechanisms for NO_3 and N_2O_5 during the DOMINO campaign: contrasts between marine, urban and continental air, Atmospheric Chemistry and Physics, 11, 10853-10870, 10.5194/acp-11-10853-2011, 2011.

Delhomme, O., Morville, S., and Millet, M.: Seasonal and diurnal variations of atmospheric concentrations of phenols and nitrophenols measured in the Strasbourg area, France, Atmospheric Pollution Research, 1, 16-22, 10.5094/apr.2010.003, 2010.

Dewald, P., Nussbaumer, C. M., Schuladen, J., Ringsdorf, A., Edtbauer, A., Fischer, H., Williams, J., Lelieveld, J., and Crowley, J. N.: Fate of the nitrate radical at the summit of a semi-rural mountain site in Germany assessed with direct reactivity measurements, Atmospheric Chemistry and Physics, 22, 7051-7069, 10.5194/acp-22-7051-2022, 2022.

Edwards, P. M., Aikin, K. C., Dube, W. P., Fry, J. L., Gilman, J. B., de Gouw, J. A., Graus, M. G., Hanisco, T. F., Holloway, J., Huber, G., Kaiser, J., Keutsch, F. N., Lerner, B. M., Neuman, J. A., Parrish, D. D., Peischl, J., Pollack, I. B., Ravishankara, A. R., Roberts, J. M., Ryerson, T. B., Trainer, M., Veres, P. R., Wolfe, G. M., Warneke, C., and Brown, S. S.: Transition from high- to low-NO_x control of night-time oxidation in the southeastern US, Nat Geosci, 10, 490-+, 10.1038/Ngeo2976, 2017.

Evans, M. J. and Jacob, D. J.: Impact of new laboratory studies of N_2O_5 hydrolysis on global model budgets of tropospheric nitrogen oxides, ozone, and OH, Geophysical Research Letters, 32, Artn L09813, Doi 10.1029/2005gl022469, 2005.

Finlayson-Pitts, B. J., James N.: Chemistry of the upper and lower atmosphere: theory, experiments and applications, Academic Press, Calif2000.

735 Fuentes., J. D., Lerdau., M., and Atkinson., R.:
736   Biogenic_hydrocarbons_in_the_atmospheric_Boundary_A review, B Am Meteorol
737   Soc, 2000.

738 Geyer, A., Alicke, B., Konrad, S., Schmitz, T., Stutz, J., and Platt, U.: Chemistry and
739   oxidation capacity of the nitrate radical in the continental boundary layer near Berlin,
740   Journal of Geophysical Research-Atmospheres, 106, 8013-8025, Doi
741   10.1029/2000jd900681, 2001.

742 Gu, S., Guenther, A., and Faiola, C.: Effects of Anthropogenic and Biogenic Volatile
743   Organic Compounds on Los Angeles Air Quality, Environ Sci Technol, 55, 12191-
744   12201, 10.1021/acs.est.1c01481, 2021.

745 Hallquist, M., Stewart, D. J., Stephenson, S. K., and Cox, R. A.: Hydrolysis of N_2O_5 on
746   sub-micron sulfate aerosols, Phys Chem Chem Phys, 5, 3453-3463, Doi
747   10.1039/B301827j, 2003.

748 Ian Barnes, Jens Hjorth, and Mihalopoulos, N.: Dimethyl Sulfide and Dimethyl Sulfoxide
749   and Their Oxidation in the Atmosphere, Chem Rev, 2006.

750 Kane, S. M., Caloz, F., and Leu, M. T.: Heterogeneous uptake of gaseous N_2O_5 by
751     $(NH_4)(2)SO_4$, NH_4HSO_4, and H_2SO_4 aerosols, J Phys Chem A, 105, 6465-6470, Doi
752   10.1021/Jp010490x, 2001.

753 Kiendler-Scharr, A., Mensah, A. A., Friese, E., Topping, D., Nemitz, E., Prevot, A. S. H.,
754   Aijala, M., Allan, J., Canonaco, F., Canagaratna, M., Carbone, S., Crippa, M., Dall
755   Osto, M., Day, D. A., De Carlo, P., Di Marco, C. F., Elbern, H., Eriksson, A., Freney,
756   E., Hao, L., Herrmann, H., Hildebrandt, L., Hillamo, R., Jimenez, J. L., Laaksonen,
757   A., McFiggans, G., Mohr, C., O'Dowd, C., Otjes, R., Ovadnevaite, J., Pandis, S. N.,
758   Poulain, L., Schlag, P., Sellegri, K., Swietlicki, E., Tiitta, P., Vermeulen, A., Wahner,
759   A., Worsnop, D., and Wu, H. C.: Ubiquity of organic nitrates from nighttime chemistry
760   in the European submicron aerosol, Geophysical Research Letters, 43, 7735-7744,
761   10.1002/2016gl069239, 2016.

762 Li, Z., Xie, P., Hu, R., Wang, D., Jin, H., Chen, H., Lin, C., and Liu, W.: Observations of
763   N_2O_5 and NO_3 at a suburban environment in Yangtze river delta in China: Estimating
764   heterogeneous N_2O_5 uptake coefficients, J Environ Sci (China), 95, 248-255,
765   10.1016/j.jes.2020.04.041, 2020.

766 Liebmann, J., Karu, E., Sobanski, N., Schuladen, J., Ehn, M., Schallhart, S., Quelever, L.,
767   Hellen, H., Hakola, H., Hoffmann, T., Williams, J., Fischer, H., Lelieveld, J., and
768   Crowley, J. N.: Direct measurement of NO_3 radical reactivity in a boreal forest,
769   Atmospheric Chemistry and Physics, 18, 3799-3815, 10.5194/acp-18-3799-2018,
770   2018a.

771 Liebmann, J. M., Muller, J. B. A., Kubistin, D., Claude, A., Holla, R., Plass-Dulmer, C.,
772   Lelieveld, J., and Crowley, J. N.: Direct measurements of NO_3 reactivity in and above
773   the boundary layer of a mountaintop site: identification of reactive trace gases and

774   comparison with OH reactivity, Atmospheric Chemistry and Physics, 18, 12045-
775   12059, 10.5194/acp-18-12045-2018, 2018b.

776 Lin, C., Hu, R., Xie, P., Lou, S., Zhang, G., Tong, J., Liu, J., and Liu, W.: Nocturnal
777   atmospheric chemistry of NO_3 and N_2O_5 over Changzhou in the Yangtze River Delta
778   in China, J Environ Sci (China), 114, 376-390, 10.1016/j.jes.2021.09.016, 2022.

779 Liu, X., Lyu, X., Wang, Y., Jiang, F., and Guo, H.: Intercomparison of O_3 formation and
780   radical chemistry in the past decade at a suburban site in Hong Kong, Atmospheric
781   Chemistry and Physics, 19, 5127-5145, 10.5194/acp-19-5127-2019, 2019.

782 Liu, X. G., Gu, J. W., Li, Y. P., Cheng, Y. F., Qu, Y., Han, T. T., Wang, J. L., Tian, H. Z.,
783   Chen, J., and Zhang, Y. H.: Increase of aerosol scattering by hygroscopic growth:
784   Observation, modeling, and implications on visibility, Atmospheric Research, 132,
785   91-101, 10.1016/j.atmosres.2013.04.007, 2013.

786 Lu, K. D., Zhang, Y. H., Su, H., Brauers, T., Chou, C. C., Hofzumahaus, A., Liu, S. C., Kita,
787   K., Kondo, Y., Shao, M., Wahner, A., Wang, J. L., Wang, X. S., and Zhu, T.: Oxidant
788   (O_3 + NO_2) production processes and formation regimes in Beijing, Journal of
789   Geophysical Research-Atmospheres, 115, Artn D07303, 10.1029/2009jd012714,
790   2010.

791 Lu, X., Qin, M., Xie, P., Duan, J., Fang, W., and Liu, W.: Observation of ambient NO_3
792   radicals by LP-DOAS at a rural site in North China Plain, Sci Total Environ, 804,
793   149680, 10.1016/j.scitotenv.2021.149680, 2022.

794 Lüttke, J., Scheer, V., Levsen, K., Wünsch, G., Cape, J. N., Hargreaves, K. J., Storeton-
795   West, R. L., Acker, K., Wieprecht, W., and Jones, B.: Occurrence and formation of
796   nitrated phenols in and out of cloud, Atmospheric Environment, 31, 2637-2648, 1997.

797 McMurry, P. H., Woo, K. S., Weber, R., Chen, D. R., and Pui, D. Y. H.: Size distributions
798   of 3-10 nm atmospheric particles: implications for nucleation mechanisms,
799   Philosophical Transactions of the Royal Society a-Mathematical Physical and
800   Engineering Sciences, 358, 2625-2642, 10.1098/rsta.2000.0673, 2000.

801 Mogensen, D., Gierens, R., Crowley, J. N., Keronen, P., Smolander, S., Sogachev, A.,
802   Nolscher, A. C., Zhou, L., Kulmala, M., Tang, M. J., Williams, J., and Boy, M.:
803   Simulations of atmospheric OH, O_3 and NO_3 reactivities within and above the boreal
804   forest, Atmospheric Chemistry and Physics, 15, 3909-3932, 10.5194/acp-15-3909-
805   2015, 2015.

806 Morgan, W. T., Ouyang, B., Allan, J. D., Aruffo, E., Di Carlo, P., Kennedy, O. J., Lowe, D.,
807   Flynn, M. J., Rosenberg, P. D., Williams, P. I., Jones, R., McFiggans, G. B., and Coe,
808   H.: Influence of aerosol chemical composition on N_2O_5 uptake: airborne regional
809   measurements in northwestern Europe, Atmospheric Chemistry and Physics, 15, 973-
810   990, DOI 10.5194/acp-15-973-2015, 2015.

811 Ng, N. L., Brown, S. S., Archibald, A. T., Atlas, E., Cohen, R. C., Crowley, J. N., Day, D.
812   A., Donahue, N. M., Fry, J. L., Fuchs, H., Griffin, R. J., Guzman, M. I., Herrmann, H.,

Hodzic, A., Iinuma, Y., Jimenez, J. L., Kiendler-Scharr, A., Lee, B. H., Luecken, D. J., Mao, J. Q., McLaren, R., Mutzel, A., Osthoff, H. D., Ouyang, B., Picquet-Varrault, B., Platt, U., Pye, H. O. T., Rudich, Y., Schwantes, R. H., Shiraiwa, M., Stutz, J., Thornton, J. A., Tilgner, A., Williams, B. J., and Zaveri, R. A.: Nitrate radicals and biogenic volatile organic compounds: oxidation, mechanisms, and organic aerosol, Atmospheric Chemistry and Physics, 17, 2103-2162, 10.5194/acp-17-2103-2017, 2017.

Niu, Y. B., Zhu, B., He, L. Y., Wang, Z., Lin, X. Y., Tang, M. X., and Huang, X. F.: Fast Nocturnal Heterogeneous Chemistry in a Coastal Background Atmosphere and Its Implications for Daytime Photochemistry, Journal of Geophysical Research: Atmospheres, 127, 10.1029/2022jd036716, 2022.

Osthoff, H. D., Pilling, M. J., Ravishankara, A. R., and Brown, S. S.: Temperature dependence of the NO_3 absorption cross-section above 298 K and determination of the equilibrium constant for $NO_3 + NO_2 \rightarrow N_2O_5$ at atmospherically relevant conditions, Phys Chem Chem Phys, 9, 5785-5793, 10.1039/b709193a, 2007.

Osthoff, H. D., Roberts, J. M., Ravishankara, A. R., Williams, E. J., Lerner, B. M., Sommariva, R., Bates, T. S., Coffman, D., Quinn, P. K., Dibb, J. E., Stark, H., Burkholder, J. B., Talukdar, R. K., Meagher, J., Fehsenfeld, F. C., and Brown, S. S.: High levels of nitryl chloride in the polluted subtropical marine boundary layer, Nat Geosci, 1, 324-328, Doi 10.1038/Ngeo177, 2008.

Riedel, T. P., Bertram, T. H., Crisp, T. A., Williams, E. J., Lerner, B. M., Vlasenko, A., Li, S. M., Gilman, J., de Gouw, J., Bon, D. M., Wagner, N. L., Brown, S. S., and Thornton, J. A.: Nitryl Chloride and Molecular Chlorine in the Coastal Marine Boundary Layer, Environmental Science & Technology, 46, 10463-10470, 10.1021/es204632r, 2012.

Riedel, T. P., Wolfe, G. M., Danas, K. T., Gilman, J. B., Kuster, W. C., Bon, D. M., Vlasenko, A., Li, S. M., Williams, E. J., Lerner, B. M., Veres, P. R., Roberts, J. M., Holloway, J. S., Lefer, B., Brown, S. S., and Thornton, J. A.: An MCM modeling study of nitryl chloride ($ClNO_2$) impacts on oxidation, ozone production and nitrogen oxide partitioning in polluted continental outflow, Atmospheric Chemistry and Physics, 14, 3789-3800, 10.5194/acp-14-3789-2014, 2014.

Rosati, B., Isokääntä, S., Christiansen, S., Jensen, M. M., Moosakutty, S. P., Wollesen de Jonge, R., Massling, A., Glasius, M., Elm, J., Virtanen, A., and Bilde, M.: Hygroscopicity and CCN potential of DMS-derived aerosol particles, Atmospheric Chemistry and Physics, 22, 13449-13466, 10.5194/acp-22-13449-2022, 2022.

Tang, M. J., Schuster, G., and Crowley, J. N.: Heterogeneous reaction of N2O5 with illite and Arizona test dust particles, Atmospheric Chemistry and Physics, 14, 245-254, DOI 10.5194/acp-14-245-2014, 2014.

Tham, Y. J., Wang, Z., Li, Q., Wang, W., Wang, X., Lu, K., Ma, N., Yan, C., Kecorius, S., Wiedensohler, A., Zhang, Y., and Wang, T.: Heterogeneous N_2O_5 uptake coefficient

and production yield of ClNO$_2$ in polluted northern China: roles of aerosol water content and chemical composition, Atmos. Chem. Phys., 18, 13155-13171, 10.5194/acp-18-13155-2018, 2018.

Tham, Y. J., Wang, Z., Li, Q. Y., Yun, H., Wang, W. H., Wang, X. F., Xue, L. K., Lu, K. D., Ma, N., Bohn, B., Li, X., Kecorius, S., Gross, J., Shao, M., Wiedensohler, A., Zhang, Y. H., and Wang, T.: Significant concentrations of nitryl chloride sustained in the morning: investigations of the causes and impacts on ozone production in a polluted region of northern China, Atmospheric Chemistry and Physics, 16, 14959-14977, 10.5194/acp-16-14959-2016, 2016.

Thornton, J. A., Kercher, J. P., Rie De L, T. P., Wagner, N. L., Cozic, J., Holloway, J. S., Dubé, W., Wolfe, G. M., Quinn, P. K., and Middlebrook, A. M.: A large atomic chlorine source inferred from mid-continental reactive nitrogen chemistry, Nature, 464, 271-274, 2010.

Vrekoussis, M., Mihalopoulos, N., Gerasopoulos, E., Kanakidou, M., Crutzen, P. J., and Lelieveld, J.: Two-years of NO$_3$ radical observations in the boundary layer over the Eastern Mediterranean, Atmospheric Chemistry and Physics, 7, 315-327, 2007.

Vrekoussis, M., Kanakidou, M., Mihalopoulos, N., Crutzen, P. J., Lelieveld, J., Perner, D., Berresheim, H., and Baboukas, E.: Role of the NO$_3$ radicals in oxidation processes in the eastern Mediterranean troposphere during the MINOS campaign, Atmospheric Chemistry and Physics, 4, 169-182, 2004.

Wagner, N. L., Riedel, T. P., Young, C. J., Bahreini, R., Brock, C. A., Dube, W. P., Kim, S., Middlebrook, A. M., Ozturk, F., Roberts, J. M., Russo, R., Sive, B., Swarthout, R., Thornton, J. A., VandenBoer, T. C., Zhou, Y., and Brown, S. S.: N$_2$O$_5$ uptake coefficients and nocturnal NO$_2$ removal rates determined from ambient wintertime measurements, Journal of Geophysical Research-Atmospheres, 118, 9331-9350, Doi 10.1002/Jgrd.50653, 2013.

Wang, H., Chen, J., and Lu, K.: Development of a portable cavity-enhanced absorption spectrometer for the measurement of ambient NO$_3$ and N$_2$O$_5$: experimental setup, lab characterizations, and field applications in a polluted urban environment, Atmos Meas Tech, 10, 1465-1479, 10.5194/amt-10-1465-2017, 2017a.

Wang, H., Chen, T., and Lu, K.: Measurement of NO$_3$ and N$_2$O$_5$ in the Troposphere, Progress in Chemistry, 27, 963-976, 10.7536/pc141230, 2015.

Wang, H., Lu, K., Chen, S., Li, X., Zeng, L., Hu, M., and Zhang, Y.: Characterizing nitrate radical budget trends in Beijing during 2013–2019, Science of The Total Environment, 795, 10.1016/j.scitotenv.2021.148869, 2021.

Wang, H., Wang, H., Lu, X., Lu, K., Zhang, L., Tham, Y. J., Shi, Z., Aikin, K., Fan, S., Brown, S. S., and Zhang, Y.: Increased night-time oxidation over China despite widespread decrease across the globe, Nat Geosci, 10.1038/s41561-022-01122-x, 2023.

891   Wang, H., Lyu, X., Guo, H., Wang, Y., Zou, S., Ling, Z., Wang, X., Jiang, F., Zeren, Y., Pan,
892   W., Huang, X., and Shen, J.: WS-Ozone pollution around a coastal region of South
893   China Sea: interaction between marine and continental air, Atmospheric Chemistry
894   and Physics, 18, 4277-4295, 10.5194/acp-18-4277-2018, 2018a.
895   Wang, H., Chen, X., Lu, K., Hu, R., Li, Z., Wang, H., Ma, X., Yang, X., Chen, S., Dong,
896   H., Liu, Y., Fang, X., Zeng, L., Hu, M., and Zhang, Y.: NO_3 and N_2O_5 chemistry at a
897   suburban site during the EXPLORE-YRD campaign in 2018, Atmospheric
898   Environment, 224, 10.1016/j.atmosenv.2019.117180, 2020a.
899   Wang, H., Chen, X., Lu, K., Tan, Z., Ma, X., Wu, Z., Li, X., Liu, Y., Shang, D., Wu, Y.,
900   Zeng, L., Hu, M., Schmitt, S., Kiendler-Scharr, A., Wahner, A., and Zhang, Y.:
901   Wintertime N_2O_5 uptake coefficients over the North China Plain, Science Bulletin, 65,
902   765-774, 10.1016/j.scib.2020.02.006, 2020b.
903   Wang, H., Lu, K., Guo, S., Wu, Z., Shang, D., Tan, Z., Wang, Y., Le Breton, M., Lou, S.,
904   Tang, M., Wu, Y., Zhu, W., Zheng, J., Zeng, L., Hallquist, M., Hu, M., and Zhang, Y.:
905   Efficient N_2O_5 uptake and NO_3 oxidation in the outflow of urban Beijing,
906   Atmospheric Chemistry and Physics, 18, 9705-9721, 10.5194/acp-18-9705-2018,
907   2018b.
908   Wang, H., Lu, K., Chen, X., Zhu, Q., Chen, Q., Guo, S., Jiang, M., Li, X., Shang, D., Tan,
909   Z., Wu, Y., Wu, Z., Zou, Q., Zheng, Y., Zeng, L., Zhu, T., Hu, M., and Zhang, Y.: High
910   N_2O_5 Concentrations Observed in Urban Beijing: Implications of a Large Nitrate
911   Formation Pathway, Environmental Science & Technology Letters, 4, 416-420,
912   10.1021/acs.estlett.7b00341, 2017b.
913   Wang, H., Yuan, B., Zheng, E., Zhang, X., Wang, J., Lu, K., Ye, C., Yang, L., Huang, S.,
914   Hu, W., Yang, S., Peng, Y., Qi, J., Wang, S., He, X., Chen, Y., Li, T., Wang, W.,
915   Huangfu, Y., Li, X., Cai, M., Wang, X., and Shao, M.: Formation and impacts of nitryl
916   chloride in Pearl River Delta, Atmospheric Chemistry and Physics, 22, 14837-14858,
917   10.5194/acp-22-14837-2022, 2022.
918   Wang, S. S., Shi, C. Z., Zhou, B., Zhao, H., Wang, Z. R., Yang, S. N., and Chen, L. M.:
919   Observation of NO_3 radicals over Shanghai, China, Atmospheric Environment, 70,
920   401-409, DOI 10.1016/j.atmosenv.2013.01.022, 2013.
921   Wang, X. F., Wang, H., Xue, L. K., Wang, T., Wang, L. W., Gu, R. R., Wang, W. H., Tham,
922   Y. J., Wang, Z., Yang, L. X., Chen, J. M., and Wang, W. X.: Observations of N_2O_5 and
923        $ClNO_2$ at a polluted urban surface site in North China: High N_2O_5 uptake coefficients
924   and low $ClNO_2$ product yields, Atmospheric Environment, 156, 125-134,
925   10.1016/j.atmosenv.2017.02.035, 2017c.
926   Wang, Z., Wang, W. H., Tham, Y. J., Li, Q. Y., Wang, H., Wen, L., Wang, X. F., and Wang,
927   T.: Fast heterogeneous N_2O_5 uptake and $ClNO_2$ production in power plant and
928   industrial plumes observed in the nocturnal residual layer over the North China Plain,
929   Atmospheric Chemistry and Physics, 17, 12361-12378, 10.5194/acp-17-12361-2017,

930   2017d.

931   Wang, J., Wang, H., Tham, Y. J., Ming, L., Zheng, Z., Fang, G., Sun, C., Ling, Z., Zhao, J.,
932   and Fan, S.. (2023). Measurement report: Atmospheric nitrate radical chemistry in the
933   South China Sea influenced by the urban outflow of the Pearl River Delta [Data set].
934   Zenodo. https://doi.org/10.5281/zenodo.8089100.

935   Wayne, R. P., Barnes, I., Biggs, P., Burrows, J. P., Canosamas, C. E., Hjorth, J., Lebras, G.,
936   Moortgat, G. K., Perner, D., Poulet, G., Restelli, G., and Sidebottom, H.: The Nitrate
937   Radical - Physics, Chemistry, and the Atmosphere, Atmos Environ a-Gen, 25, 1-203,
938   Doi 10.1016/0960-1686(91)90192-A, 1991.

939   Wood, E. C., Bertram, T. H., Wooldridge, P. J., and Cohen, R. C.: Measurements of N_2O_5,
940   NO_2, and O_3 east of the San Francisco Bay, 2005.

941   Xu, L., Guo, H., Boyd, C. M., Klein, M., Bougiatioti, A., Cerully, K. M., Hite, J. R.,
942   Isaacman-VanWertz, G., Kreisberg, N. M., Knote, C., Olson, K., Koss, A., Goldstein,
943   A. H., Hering, S. V., de Gouw, J., Baumann, K., Lee, S. H., Nenes, A., Weber, R. J.,
944   and Ng, N. L.: Effects of anthropogenic emissions on aerosol formation from isoprene
945   and monoterpenes in the southeastern United States (vol 112, pg 37, 2015), P Natl
946   Acad Sci USA, 112, E4506-E4507, 2015.

947   Yan, C., Tham, Y. J., Zha, Q. Z., Wang, X. F., Xue, L. K., Dai, J. N., Wang, Z., and Wang,
948   T.: Fast heterogeneous loss of N_2O_5 leads to significant nighttime NO_x removal and
949   nitrate aerosol formation at a coastal background environment of southern China,
950   Science of the Total Environment, 677, 637-647, 10.1016/j.scitotenv.2019.04.389,
951   2019.

952   Yan, Y., Wang, S., Zhu, J., Guo, Y., Tang, G., Liu, B., An, X., Wang, Y., and Zhou, B.:
953   Vertically increased NO_3 radical in the nocturnal boundary layer, Sci Total Environ,
954   763, 142969, 10.1016/j.scitotenv.2020.142969, 2021.

955   Yang, S., Yuan, B., Peng, Y., Huang, S., Chen, W., Hu, W., Pei, C., Zhou, J., Parrish, D. D.,
956   Wang, W., He, X., Cheng, C., Li, X.-B., Yang, X., Song, Y., Wang, H., Qi, J., Wang,
957   B., Wang, C., Wang, C., Wang, Z., Li, T., Zheng, E., Wang, S., Wu, C., Cai, M., Ye,
958   C., Song, W., Cheng, P., Chen, D., Wang, X., Zhang, Z., Wang, X., Zheng, J., and Shao,
959   M.: The formation and mitigation of nitrate pollution: comparison between urban and
960   suburban environments, Atmospheric Chemistry and Physics, 22, 4539-4556,
961   10.5194/acp-22-4539-2022, 2022.

962   Yu, C., Wang, Z., Xia, M., Fu, X., Wang, W., Tham, Y. J., Chen, T., Zheng, P., Li, H., Shan,
963   Y., Wang, X., Xue, L., Zhou, Y., Yue, D., Ou, Y., Gao, J., Lu, K., Brown, S. S., Zhang,
964   Y., and Wang, T.: Heterogeneous N_2O_5 reactions on atmospheric aerosols at four
965   Chinese sites: improving model representation of uptake parameters, Atmos. Chem.
966   Phys., 20, 4367-4378, 10.5194/acp-20-4367-2020, 2020.

967   Yun, H., Wang, T., Wang, W. H., Tham, Y. J., Li, Q. Y., Wang, Z., and Poon, S. C. N.:
968   Nighttime NO_x loss and $ClNO_2$ formation in the residual layer of a polluted region:

969   Insights from field measurements and an iterative box model, Science of the Total
970   Environment, 622, 727-734, 10.1016/j.scitotenv.2017.11.352, 2018a.

971 Yun, H., Wang, W. H., Wang, T., Xia, M., Yu, C., Wang, Z., Poon, S. C. N., Yue, D. L., and
972   Zhou, Y.: Nitrate formation from heterogeneous uptake of dinitrogen pentoxide during
973   a severe winter haze in southern China, Atmospheric Chemistry and Physics, 18,
974   17515-17527, 10.5194/acp-18-17515-2018, 2018b.

975 Zhou, W., Zhao, J., Ouyang, B., Mehra, A., Xu, W. Q., Wang, Y. Y., Bannan, T. J., Worrall,
976   S. D., Priestley, M., Bacak, A., Chen, Q., Xie, C. H., Wang, Q. Q., Wang, J. F., Du, W.,
977   Zhang, Y. J., Ge, X. L., Ye, P. L., Lee, J. D., Fu, P. Q., Wang, Z. F., Worsnop, D., Jones,
978   R., Percival, C. J., Coe, H., and Sun, Y. L.: Production of N_2O_5 and $ClNO_2$ in summer
979   in urban Beijing, China, Atmospheric Chemistry and Physics, 18, 11581-11597,
980   10.5194/acp-18-11581-2018, 2018.

981 Zhu, J., Wang, S., Zhang, S., Xue, R., Gu, C., and Zhou, B.: Changes in NO_3 Radical and
982   Its Nocturnal Chemistry in Shanghai From 2014 to 2021 Revealed by Long‐Term
983   Observation and a Stacking Model: Impact of China's Clean Air Action Plan, Journal
984   of Geophysical Research: Atmospheres, 127, 10.1029/2022jd037438, 2022.

985